PHYSICAL REVIEW D **95,** 014034 (2017)

# Perturbative QCD and beyond: Azimuthal angle correlations in deuteron-deuteron scattering from Bose-Einstein correlations

E. Gotsman[1,*] and E. Levin[1,2,†]

[1]*Department of Particle Physics, School of Physics and Astronomy, Raymond and Beverly Sackler Faculty of Exact Science, Tel Aviv University, Haim Levanon Street, Ramat Aviv, Tel Aviv 6997801, Israel*

[2]*Departemento de Física, Universidad Técnica Federico Santa María, and Centro Científico- Tecnológico de Valparaíso, Avenida Espana 1680, Casilla 110-V, Valparaíso, Chile*

(Received 16 November 2016; published 30 January 2017)

In this paper, we find, within the framework of perturbative QCD, that in deuteron-deuteron scattering Bose-Einstein correlations, due to production of two-parton showers, induce azimuthal angle correlations with three correlation lengths: the size of the deuteron ($R_D$), the proton radius ($R_N$), and the size of the Balitski-Fadin-Kuraev-Lipatov (BFKL) Pomeron, which is closely related to the saturation momentum ($R_c \sim 1/Q_s$). These correlations are independent of the values of rapidities of the produced gluons (long range rapidity correlations) for large rapidities ($\bar{\alpha}_S|y_1 - y_2| \geq 1$) and have no symmetry with respect to $\phi \to \pi - \phi$ ($\boldsymbol{p}_{T1} \to -\boldsymbol{p}_{T1}$). Therefore, they give rise to $v_n$ for all values of $n$, not only for even values. The contributions of the correlation lengths $R_D$ and $R_N$ crucially depend on the nonperturbative contributions, and obtaining estimates of their values requires a lot of modeling, while the correlations with $R_c \sim 1/Q_s$ have a perturbative QCD origin and can be estimated in the color glass condensate approach.

DOI: 10.1103/PhysRevD.95.014034

## I. INTRODUCTION

In this paper we continue to resurrect the old ideas of Gribov Pomeron calculus, namely that Bose-Einstein correlations lead to strong azimuthal angle correlations [1], which do not depend on the rapidity difference between measured hadrons [long range rapidity (LRR) correlations]. In the framework of QCD, these azimuthal correlations stem from the production of two-parton showers and have been rediscovered in Refs. [2,3]. In Ref. [4] it was demonstrated that Bose-Einstein correlations generate $v_n$ with even and odd $n$ values, including values which are close to the experimental values [5–15].

The goal of this paper is to show that the Bose-Einstein correlations that have been discussed in Refs. [1,4] arise naturally in the perturbative QCD approach together with ones that have been considered in Refs. [2,3]. We believe that the qualitative difference between these two approaches originates from different sources of the Bose-Einstein correlations: the two-parton-shower production in Refs. [1,4] and one-parton shower in Refs. [2,3].

Here, we consider the azimuthal correlations for deuteron-deuteron scattering at high energy. It is well known [16] (see also Ref. [17]), that Bose-Einstein correlations provide a possibility to measure the volume of interaction or, in other words, the typical sizes of the interaction. Indeed, the general formula for the Bose-Einstein correlations [16,17] takes the form

$$\frac{d^2\sigma}{dy_1 dy_2 d^2p_{T1} d^2p_{T2}}(\text{identical gluons}) \propto \langle 1 + e^{ir_\mu Q_\mu}\rangle, \quad (1)$$

where averaging $\langle \ldots \rangle$ includes the integration over $r_\mu = r_{1,\mu} - r_{2,\mu}$. For the case of $y_1 = y_2$, $Q_\mu = p_{1,\mu} - p_{2,\mu}$ simplifies to $\boldsymbol{Q} \equiv \boldsymbol{p}_{T,12} = \boldsymbol{p}_{T1} - \boldsymbol{p}_{T2}$,

One can see that Eq. (1) allows us to measure the typical $r_\mu$ for the interaction. For deuteron-deuteron scattering we expect several typical $r$: the size of the deuteron $R_D$, the nucleon size $R_N$, and the typical size, related to the saturation scale ($r_{\text{sat}} = 1/Q_s$, where $Q_s$ denotes the saturation scale [18]). In our calculation we hope to see the appearance of these scales.

It is well known that the total cross section for the deuteron-deuteron scattering can be written in the form $\sigma_{DD} = 4\sigma_{NN} - \Delta\sigma_{DD}$, where $\Delta\sigma_{DD}$ is the Glauber correction term [19], which is proportional to $1/R_D^2$, while $\sigma_{NN}$ denotes the total cross section of the nucleon-nucleon interaction. Intuition suggests that the correlation radius of the order of $R_D$ stems from the production due to the Glauber correction term (see Fig. 1)

The production of two gluons is shown in Fig. 1(a) and Fig. 1(b), where interference in the case of the generated identical gluon leads to the correlation function of Eq. (1). Generally speaking, the inclusive production of two gluons with rapidities $y_1$ and $y_2$ and transverse momenta $\boldsymbol{p}_{T1}$ and $\boldsymbol{p}_{T2}$ takes the form

*gotsman@post.tau.ac.il
†leving@post.tau.ac.il, eugeny.levin@usm.cl

 

$$\frac{d^2\sigma}{dy_1 dy_2 d^2p_{T1} d^2p_{T2}}(\text{identical gluons}) = \frac{d^2\sigma}{dy_1 dy_2 d^2p_{T1} d^2p_{T2}}(\text{different gluons})\left(\underbrace{1}_{\text{squared of diagrams}} + \underbrace{C(R_c|\boldsymbol{p}_{T1}-\boldsymbol{p}_{T2}|)}_{\text{interference diagram}}\right). \tag{2}$$

In Eq. (2) $R_c$ denotes the correlation radius (correlation length), and in the form of the correlation function, we anticipate that the production of two-parton showers leads to the double inclusive cross section, which does not depend on rapidities $y_1$ and $y_2$.

## II. BORN APPROXIMATION

### A. Bose-Einstein correlation function with radius $\propto R_D$

The simplest contribution in the Born approximation of perturbative QCD is shown in Fig. 2. The second diagram describes the interference between two-parton showers shown in Fig. 1(b).

The analytical expressions take the following forms. For the diagram of Fig. 2(a), we have

$$\begin{aligned}\frac{d^2\sigma}{dy_1 dy_2 d^2p_{T1} d^2p_{T2}}(\text{Fig.2(a)}) &\propto \int d^2Q_T G_D^2(Q_T)\int d^2k_t d^2l_T\left(\frac{I_P(\boldsymbol{k}_T,-\boldsymbol{k}_T+\boldsymbol{Q}_T)}{\boldsymbol{k}_T^2(\boldsymbol{k}-\boldsymbol{p}_1)_T^2}\Gamma_\mu(\boldsymbol{k}_T,\boldsymbol{p}_{T1})\Gamma_\mu(-\boldsymbol{k}_T+\boldsymbol{Q}_T,\boldsymbol{p}_{T1})\frac{I_P(\boldsymbol{k}_T-\boldsymbol{p}_{T1},-\boldsymbol{k}_T+\boldsymbol{p}_{T1}+\boldsymbol{Q}_T)}{(-\boldsymbol{k}+\boldsymbol{Q})_T^2(-\boldsymbol{k}+\boldsymbol{p}_1+\boldsymbol{Q})_T^2}\right)\\ &\times\left(\frac{I_P(\boldsymbol{l}_T,-\boldsymbol{l}_T-\boldsymbol{Q}_T)}{\boldsymbol{l}_T^2(\boldsymbol{l}-\boldsymbol{p}_2)_T^2}\Gamma_\nu(\boldsymbol{l}_T,\boldsymbol{p}_{T2})\Gamma_\nu(-\boldsymbol{l}_T-\boldsymbol{Q}_T,\boldsymbol{p}_{T2})\frac{I_P(\boldsymbol{l}_T-\boldsymbol{p}_{T2},-\boldsymbol{l}_T+\boldsymbol{p}_{T2}-\boldsymbol{Q}_T)}{(-\boldsymbol{l}-\boldsymbol{Q})_T^2(-\boldsymbol{l}+\boldsymbol{p}_2-\boldsymbol{Q})_T^2}\right).\end{aligned} \tag{3}$$

The interference diagram of Fig. 2(b) takes the following form

$$\begin{aligned}\frac{d^2\sigma}{dy_1 dy_2 d^2p_{T1} d^2p_{T2}}(\text{Fig.2(b)}) &\propto \int d^2Q_T G_D(Q_T)G_D(\boldsymbol{Q}_T+\boldsymbol{p}_{T,12})\\ &\times\int d^2k_T d^2l_T\left(\frac{I_P(\boldsymbol{k}_T,-\boldsymbol{k}_T+\boldsymbol{Q}_T)}{\boldsymbol{k}_T^2(\boldsymbol{k}-\boldsymbol{p}_1)_T^2}\Gamma_\mu(\boldsymbol{k}_T,\boldsymbol{p}_{T1})\Gamma_\mu(-\boldsymbol{l}_T-\boldsymbol{Q}_T,\boldsymbol{p}_{T1})\frac{I_P(\boldsymbol{k}_T-\boldsymbol{p}_{T1},-\boldsymbol{k}_T+\boldsymbol{p}_{T1}+\boldsymbol{Q}_T)}{(-\boldsymbol{l}-\boldsymbol{Q})_T^2(-\boldsymbol{l}+\boldsymbol{p}_1-\boldsymbol{Q})_T^2}\right)\\ &\times\left(\frac{I_P(\vec{l}_T,-\vec{l}_T-\vec{Q}_T)}{\vec{l}_T^2(\vec{l}-\vec{p}_2)_T^2}\Gamma_\mu(l_T,\boldsymbol{p}_{T2})\Gamma_\mu(-\boldsymbol{k}_T+\boldsymbol{Q}_T,\boldsymbol{p}_{T2})\frac{I_P(\boldsymbol{l}_T-\boldsymbol{p}_{T2},-\boldsymbol{l}_T+\boldsymbol{p}_{T2}-\boldsymbol{Q}_T)}{(-\boldsymbol{k}+\boldsymbol{Q})_T^2(-\boldsymbol{k}+\boldsymbol{p}_2+\boldsymbol{Q})_T^2}\right).\end{aligned} \tag{4}$$

The Lipatov vertices $\Gamma_\mu$ have the forms (see Ref. [18] for example)

$$\Gamma_\mu(k_T,p_{T1})=\frac{1}{p_{T1}^2}(k_T^2\boldsymbol{p}_{T1}-\boldsymbol{k}_T p_{T1}^2);\qquad \Gamma_\mu(k_{T1},p_{T2})=\frac{1}{p_{T2}^2}(k_{T1}^2\boldsymbol{p}_{T2}-\boldsymbol{k}_{T1}p_{T2}^2) \tag{5}$$

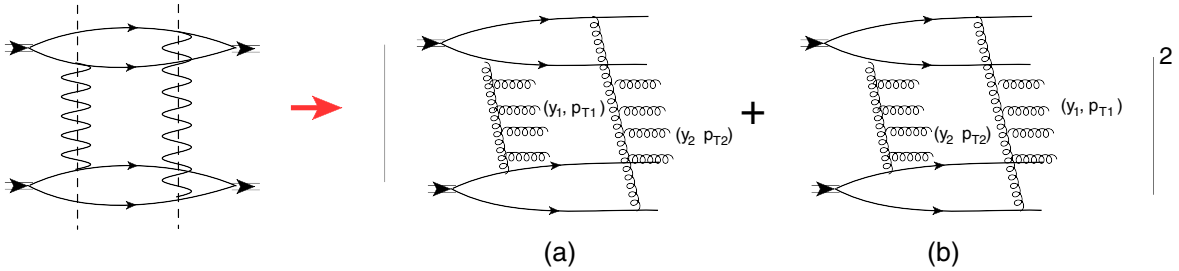


FIG. 1. The two-parton-shower production that contributes to the Glauber correction term for deuteron-deuteron scattering. The wavy lines describe the exchange of the BFKL Pomeron. Figure 1(a) and Fig. 1(b) show two diagrams that can interfere for identical gluons. The dashed lines show the cut BFKL Pomeron [20].

and

$$\Gamma_\mu(k_T,p_{T1})\Gamma_\mu(k_{T1},p_{T2})=\frac{k_{T1}^2(\boldsymbol{k}_T-\boldsymbol{p}_{T2})^2}{p_{T2}^2}+\frac{k_T^2(\boldsymbol{k}_{T1}-\boldsymbol{p}_{T1})^2}{p_{T1}^2}-Q_T^2-p_{T,12}^2\frac{k_T^2k_{T1}^2}{p_{T1}^2p_{T2}^2}, \tag{6}$$

where $\boldsymbol{p}_{T,12}=\boldsymbol{p}_{T1}-\boldsymbol{p}_{T2}$ and $\boldsymbol{k}_{T1}=\boldsymbol{k}_T-\boldsymbol{Q}_T$. One can see from Eq. (6) that

$$\Gamma_\mu(k_T,p_{T1})\Gamma_\mu(k_{T1},p_{T2})\xrightarrow{k_T\ll Q_T}k_T^2\left(1+\mathcal{O}\left(\frac{Q}{p_{T1}};\frac{k_T}{p_{T1}}\right)\right)$$
$$\Gamma_\mu(k_T,p_{T1})\Gamma_\mu(k_{T1},p_{T2})\xrightarrow{k_{T1}\ll Q_T}k_{T1}^2\left(1+\mathcal{O}\left(\frac{Q}{p_{T2}};\frac{k_{T1}}{p_{T2}}\right)\right). \tag{7}$$

$G_D(Q_T)$ is equal to

$$G_D(Q_T)=\int d^2r e^{i\boldsymbol{r}\cdot\boldsymbol{Q}_T}|\Psi_D(r)|^2, \tag{8}$$

where $r$ denotes the distance between the proton and the neutron in the deuteron. The impact factors [$I_P(\boldsymbol{k}_T,-\boldsymbol{k}_T+\boldsymbol{Q}_T)$ and others in Eq. (3) and Eq. (4)] determine the interaction of two gluons with the nucleon, and their typical momenta are about $1/R_N$.

From Eq. (8) we can see that typical $Q_T\propto 1/R_D$, where $R_D$ is the deuteron radius. In other words, $Q_T$ [and $|\boldsymbol{Q}_T+\boldsymbol{p}_{T,12}|$ in Eq. (4)] turns out to be much smaller than the values of $k_T$ and $l_T$, which are determined by the size of the nucleon ($R_N$) $k_T\approx l_T\sim 1/R_N\gg Q_T(|\boldsymbol{Q}_T+\boldsymbol{p}_{T,12}|)\sim 1/R_D$ through the impact factors $I_P$ in Eq. (3) and Eq. (4). The reason is that $R_D\gg R_N$. Neglecting $Q_T$ and $p_{T,12}$ in comparison with $k_T$ and $l_T$, we can simplify Eq. (3) and Eq. (4) to the form

$$\begin{aligned}&\frac{d^2\sigma}{dy_1dy_2d^2p_{T1}d^2p_{T2}}(\text{Fig.2(a)})+\frac{d^2\sigma}{dy_1dy_2d^2p_{T1}d^2p_{T2}}(\text{Fig.2}-\text{b})\\&\propto\frac{1}{p_{T1}^2p_{T2}^2}\int d^2Q_T\left\{G_D^2(Q_T)+\frac{1}{2(N_c^2-1)}G_D(Q_T)G_D(\boldsymbol{Q}_T+\boldsymbol{p}_{T,12})\right\}\\&\times\int d^2k_td^2l_T\left(\frac{I_P(\boldsymbol{k}_T,-\boldsymbol{k}_T)I_P(\boldsymbol{k}_T-\boldsymbol{p}_{T1},-\boldsymbol{k}_T+\boldsymbol{p}_{T1})}{\boldsymbol{k}_T^2(\boldsymbol{k}-\boldsymbol{p}_1)_T^2}\right)\\&\times\left(\frac{I_P(\boldsymbol{l}_T,-\boldsymbol{l}_T)I_P(\boldsymbol{l}_T-\boldsymbol{p}_{T2},-\boldsymbol{l}_T+\boldsymbol{p}_{T2})}{\boldsymbol{l}_T^2(\boldsymbol{l}-\boldsymbol{p}_2)_T^2}\right).\end{aligned} \tag{9}$$

In Eq. (9) we consider $p_1=p_2$ for the expressions in (…). Note that the interference diagram of Fig. 2(b) contributes when the polarizations of the produced gluons are the same, this fact is reflected in Eq. (4) by the same indices of Lipatov vertices. In Eq. (9) we replace

$$\begin{aligned}&\Gamma_\mu(\boldsymbol{k}_T,\boldsymbol{p}_{T1})\Gamma_\mu(-\boldsymbol{l}_T-\boldsymbol{Q}_T,\boldsymbol{p}_{T1})\Gamma_\mu(\boldsymbol{l}_T,\boldsymbol{p}_{T2})\Gamma_\mu(-\boldsymbol{k}_T+\boldsymbol{Q}_T,\boldsymbol{p}_{T2})\\&\quad\to\frac{1}{2}\Gamma_\mu(\boldsymbol{k}_T,\boldsymbol{p}_{T1})\Gamma_\mu(-\boldsymbol{k}_T+\boldsymbol{Q}_T,\boldsymbol{p}_{T2})\Gamma_\nu(\boldsymbol{l}_T,\boldsymbol{p}_{T2})\Gamma_\nu(-\boldsymbol{l}_T-\boldsymbol{Q}_T,\boldsymbol{p}_{T1})\end{aligned} \tag{10}$$

$$\begin{aligned}&\xrightarrow{Q_T,p_{T,12}\ll k_t,l_T}\frac{1}{2}\Gamma_\mu(\boldsymbol{k}_T,\boldsymbol{p}_{T1})\Gamma_\mu(-\boldsymbol{k}_T,\boldsymbol{p}_{T1})\Gamma_\nu(\boldsymbol{l}_T,\boldsymbol{p}_{T2})\Gamma_\nu(-\boldsymbol{l}_T,\boldsymbol{p}_{T2})\\&=\frac{1}{2}\frac{1}{p_{T1}^2p_{T2}^2}k_T^2(\boldsymbol{k}-\boldsymbol{p}_1)_T^2l_T^2(\boldsymbol{l}-\boldsymbol{p}_2)_T^2.\end{aligned} \tag{11}$$

Factor $1/(N_c^2-1)$ in Eq. (9) reflects that identical gluons have the same colors ($N_c$ is the number of colors).

Finally, the correlation function $C(R_c|\boldsymbol{p}_{T1}-\boldsymbol{p}_{T2}|)$ in Eq. (2) is equal to

$$C(R_Dp_{T,12})=\frac{1}{2(N_C^2-1)}\frac{\int d^2Q_TG_D(Q_T)G_D(|\boldsymbol{Q}_T+\boldsymbol{p}_{T,12}|)}{\int d^2Q_TG_D^2(Q_T)}. \tag{12}$$

### B. Bose-Einstein correlation function with radius $\propto R_N$: Glauber corrections

In this subsection we show that the Glauber corrections due to the interaction of one nucleon with two nucleons of the deuteron, shown in Fig. 3, lead to a correlation radius of the order of $R_N$. In the diagram of Fig. 3(a), $Q_T$ is of the order of $1/R_D$; therefore, it is much smaller that the typical values of $k_T$ and $l_T$, which are of the order of $1/R_N$. Hence, the contribution of this diagram is similar to Eq. (9), namely,

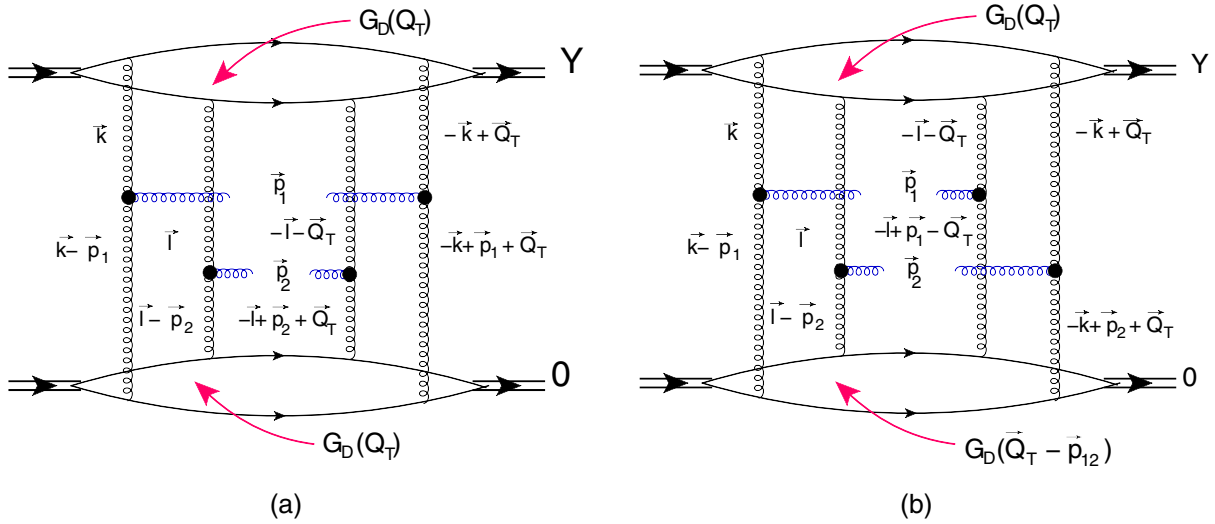


FIG. 2. The double inclusive production of two gluons with rapidities $y_1$ and $y_2$ and transverse momenta $\boldsymbol{p}_{T1}$ and $\boldsymbol{p}_{T2}$ in the Born Approximation of perturbative QCD. Figure 2(a) corresponds to the square of the diagrams of Fig. 1. The interference diagram of Fig. 2(b) gives the correlation function $C(R_D|\boldsymbol{p}_{T1}-\boldsymbol{p}_{T2}|)$ of Eq. (2). The solid lines denote nucleons in the deuterons, which are specified by double lines.

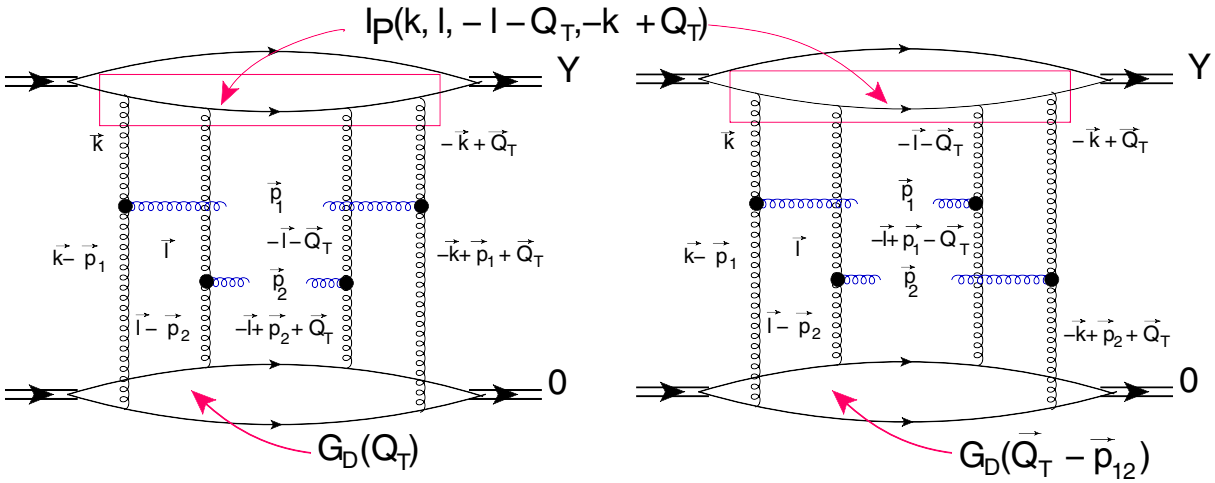


FIG. 3. The double inclusive production of two gluons with rapidities $y_1$ and $y_2$ and transverse momenta $\boldsymbol{p}_{T1}$ and $\boldsymbol{p}_{T2}$ in the Born Approximation of perturbative QCD. Figure. 3(a) corresponds to the square of the diagram of Fig. 1. The interference diagram of Fig. 3(b) yields the correlation function $C(R_N|\boldsymbol{p}_{T1}-\boldsymbol{p}_{T2}|)$ of Eq. (2). The solid lines denote nucleons in the deuterons, which are illustrated by double lines.

$$\frac{d^2\sigma}{dy_1 dy_2 d^2p_{T1} d^2p_{T2}}\,(\text{Fig.3(a)})$$
$$\propto \frac{1}{p_{T1}^2 p_{T2}^2}\int d^2Q_T G_D(Q_T)$$
$$\times \int d^2k_T d^2l_T I_P(\boldsymbol{k}_T,\boldsymbol{l}_T,-\boldsymbol{l}_T,-\boldsymbol{k}_T)$$
$$\times \frac{I_P(\boldsymbol{k}_T-\boldsymbol{p}_{T1},-\boldsymbol{k}_T+\boldsymbol{p}_{T1})I_P(\boldsymbol{l}_T-\boldsymbol{p}_{T2},-\boldsymbol{l}_T+\boldsymbol{p}_{T2})}{\boldsymbol{k}_T^2(\boldsymbol{k}-\boldsymbol{p}_1)_T^2\boldsymbol{l}_T^2(\boldsymbol{l}-\boldsymbol{p}_2)_T^2}. \tag{12}$$

Unfortunately, we cannot treat the impact factors $I_P$ theoretically in the case of nucleons. The phenomenological approach to $I_P$ has been discussed in Refs. [4,21], and we will return to this below. For the moment we replace the nucleon with the state of a heavy quark and antiquark (onium) to study the key features of the impact factors in the framework of perturbative QCD (see Fig. 4). Introducing the form factor of the onium in the form

$$F(Q_T) = \int d^2r e^{i\frac{1}{2}\boldsymbol{Q}_T\cdot\boldsymbol{r}}|\Psi_{\text{onium}}(r)|^2, \tag{13}$$

we can express the impact factor in the form

$$I_P(\boldsymbol{k}_T,-\boldsymbol{k}_T+\boldsymbol{Q}_T) = F(\boldsymbol{Q}_T) - F(2\boldsymbol{k}_T+\boldsymbol{Q}_T); \tag{14}$$

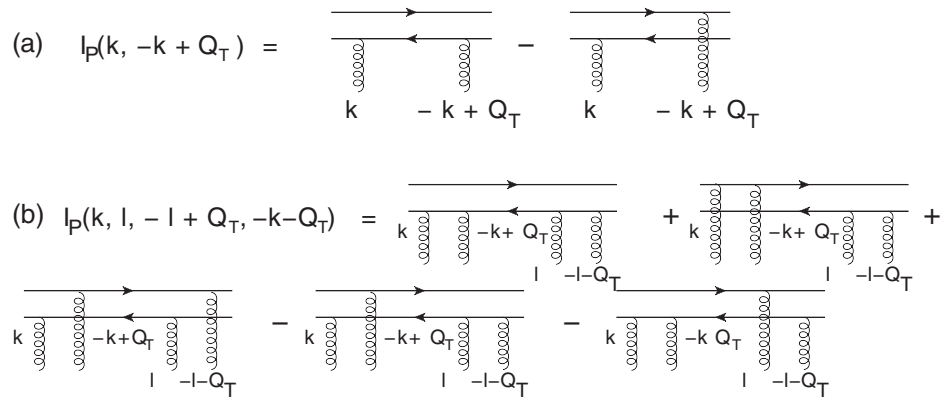


FIG. 4. The impact factors for onium for $R_N k_T > 1$, $R_N l_T > 1$, and $R_N Q_T > 1$. Figure 4(a) describes the interaction of two gluons with the onium. Figure 4(b) shows the impact factor for the interaction of four gluons with the onium.

$$I_P(\boldsymbol{k}_T,\boldsymbol{l}_T,-\boldsymbol{l}_T+\boldsymbol{Q}_T,-\boldsymbol{k}_T+\boldsymbol{Q}_T) = 1+F(2\boldsymbol{Q}_T)+F(2(\boldsymbol{k}_T+\boldsymbol{l}_T))+F(2(\boldsymbol{k}_T-\boldsymbol{l}_T-\boldsymbol{Q}_T)) - F(2\boldsymbol{k}_T)-F(2(\boldsymbol{k}_T-\boldsymbol{Q}_T))-F(2\boldsymbol{l}_T)-F(2(\boldsymbol{l}_T+\boldsymbol{Q}_T)). \tag{15}$$

In Eq. (13) the impact factors are equal to

$$I_P(\boldsymbol{k}_T,-\boldsymbol{k}_T) = 1-F(2\boldsymbol{k}_T); \quad I_P(\boldsymbol{l}_T,-\boldsymbol{l}_T) = 1-F(2\boldsymbol{l}_T); \tag{16}$$

$$I_P(\boldsymbol{k}_T,\boldsymbol{l}_T,-\boldsymbol{l}_T,-\boldsymbol{k}_T) = 2+F(2(\boldsymbol{k}_T+\boldsymbol{l}_T))+F(2(\boldsymbol{k}_T-\boldsymbol{l}_T)) - F(2\boldsymbol{k}_T)-F(2(\boldsymbol{k}_T)) - F(2\boldsymbol{l}_T)-F(2(\boldsymbol{l}_T)). \tag{17}$$

The integration over $k_T$ and $l_T$ leads to typical values of $k_T \sim 1/R_N$ and $l_T \sim 1/R_N$, and it does not generate azimuthal angle correlations. Indeed, this is clear from the following features of $I_P$ from Eq. (17):

$$\begin{aligned} &R_N k_T \ll 1, R_N l_T \ll 1; && I_P(\boldsymbol{k}_T,\boldsymbol{l}_T,-\boldsymbol{l}_T,-\boldsymbol{k}_T) \propto k_T^2 l_T^2;\\ &R_N k_T \ll 1, R_N l_T \gg 1; && I_P(\boldsymbol{k}_T,\boldsymbol{l}_T,-\boldsymbol{l}_T,-\boldsymbol{k}_T) \propto k_T^2;\\ &R_N k_T \gg 1, R_N l_T \ll 1; && I_P(\boldsymbol{k}_T,\boldsymbol{l}_T,-\boldsymbol{l}_T,-\boldsymbol{k}_T) \propto l_T^2;\\ &R_N k_T \gg 1, R_N l_T \gg 1; && I_P(\boldsymbol{k}_T,\boldsymbol{l}_T,-\boldsymbol{l}_T,-\boldsymbol{k}_T) \propto 1. \end{aligned} \tag{18}$$

In the diagram of Fig. 3(b) one can see that $G_D(\boldsymbol{Q}_T-\boldsymbol{p}_{12})$ regulates that $|\boldsymbol{Q}_T-\boldsymbol{p}_{12}|$ is of the order of $1/R_D$. This means that we can put $\boldsymbol{Q}_T=\boldsymbol{p}_{12}$ in all parts of diagrams, since the typical values of $k_T$ and $l_T$ are about $1/R_N \gg 1/R_D$. Therefore, the diagram of Fig. 3(b) can be reduced to the form

$$\begin{aligned} \frac{d^2\sigma}{dy_1 dy_2 d^2p_{T1} d^2p_{T2}}(\text{Fig.3(b)}) \propto& \frac{1}{p_{T1}^2 p_{T2}^2}\int d^2Q_T G_D(\boldsymbol{Q}_T-\boldsymbol{p}_{12})\\ &\times\int d^2k_T d^2l_T I_P(\boldsymbol{k}_T,\boldsymbol{l}_T,-\boldsymbol{l}_T-\boldsymbol{p}_{12},-\boldsymbol{k}_T+\boldsymbol{p}_{12}) I_P(\boldsymbol{k}_T-\boldsymbol{p}_{T1},-\boldsymbol{k}_T+\boldsymbol{p}_{T1}) I_P(\boldsymbol{l}_T-\boldsymbol{p}_{T2},-\boldsymbol{l}_T+\boldsymbol{p}_{T2})\\ &\times\left\{\left(\frac{1}{(\boldsymbol{k}-\boldsymbol{p}_1)_T^2(\boldsymbol{l}+\boldsymbol{p}_{12})_T^2}+\frac{1}{k_T^2(\boldsymbol{l}-\boldsymbol{p}_2)_T^2}\right)-\frac{(\boldsymbol{l}-\boldsymbol{k}+\boldsymbol{p}_{12})_T^2 p_{T,1}^2}{k_T^2(\boldsymbol{k}-\boldsymbol{p}_1)_T^2(\boldsymbol{l}-\boldsymbol{p}_2)_T^2(\boldsymbol{l}+\boldsymbol{p}_{12})^2}\right\}\\ &\times\left\{\left(\frac{1}{(\boldsymbol{l}-\boldsymbol{p}_2)_T^2(\boldsymbol{k}-\boldsymbol{p}_{12})_T^2}+\frac{1}{l_T^2(\boldsymbol{k}-\boldsymbol{p}_1)_T^2}\right)-\frac{(\boldsymbol{l}-\boldsymbol{k}+\boldsymbol{p}_{12})_T^2 p_{T,2}^2}{l_T^2(\boldsymbol{l}-\boldsymbol{p}_2)_T^2(\boldsymbol{k}-\boldsymbol{p}_1)_T^2(\boldsymbol{k}-\boldsymbol{p}_{12})^2}\right\}. \end{aligned} \tag{19}$$

The largest contributions to the integrals over $k_T$ and $l_T$ lead to the logarithmically large terms, which are proportional to $\ln(p_{T1}^2R_N^2)\ln(p_{T2}^2R_N^2)$. These contributions stem from the terms which are proportional to $1/((\boldsymbol{k}-\boldsymbol{p}_1)_T^2)^2$ and to $1/((\boldsymbol{l}-\boldsymbol{p}_2)_T^2)^2$. We consider the kinematic region in the integration over $k_T$ and $l_T$, where $\boldsymbol{k}_T-\boldsymbol{p}_{T1}\equiv\boldsymbol{k}_1\to 0$ and $\boldsymbol{l}_T-\boldsymbol{p}_{T2}\equiv\boldsymbol{l}_2\to 0$. For small $k_1 \ll p_{T2}$ and $l_2 \ll p_{T1}$, the product of curly brackets is equal to

$$\frac{1}{p_{T1}^2}\left\{\frac{1}{k_1^2}+\frac{1}{l_1^2}-\frac{(\boldsymbol{k}_1-\boldsymbol{l}_2)^2}{k_1^2 l_2^2}\right\}\frac{1}{p_{T2}^2}\left\{\frac{1}{k_1^2}+\frac{1}{l_1^2}-\frac{(\boldsymbol{k}_1-\boldsymbol{l}_2)^2}{k_1^2 l_2^2}\right\} = \frac{4(\boldsymbol{k}_1\cdot\boldsymbol{l}_2)^2}{p_{T1}^2 p_{T2}^2 k_1^4 l_2^4} \xrightarrow{\text{after integration over angle}} \frac{2}{p_{T1}^2 p_{T2}^2 k_1^2 l_2^2}. \tag{20}$$

For $R_N k_1 \ll 1$, $I_P(\boldsymbol{k}_T-\boldsymbol{p}_{T1},-\boldsymbol{k}_T+\boldsymbol{p}_{T1}) \propto k_1^2$, and the integral over $k_1$ gives a small contribution of the order of $1/(R_N^2 p_{T1}^2)$. Recall that we can use the perturbative QCD

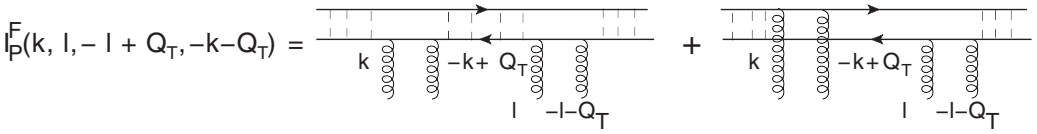


FIG. 5. The impact factors for onium for $R_N k_T > 1$, $R_N l_T > 1$, and $R_N Q_T \leq 1$. The dashed lines denote the Coulomb gluons that form the onium-bound state.

approach only if $R_N p_{T1} \gg 1$ and $R_N p_{T2} \gg 1$. Therefore, the main contribution occurs from the region of integration $(1/R_N^2) \ll k_1 \ll p_{T2}$ and $(1/R_N^2) \ll l_1 \ll p_{T1}$. Integration in this region leads to the contribution

$$\frac{d^2\sigma}{dy_1 dy_2 d^2p_{T1} d^2p_{T2}}(\text{Fig.3(b)}) \propto \frac{1}{p_{T1}^4 p_{T2}^4} \ln\left(p_{T1}^2 R_N^2\right) \ln\left(p_{T2}^2 R_N^2\right) \int d^2Q_T G_D(\boldsymbol{Q}_T - \boldsymbol{p}_{12}) \times I_P(\boldsymbol{p}_{T1}, \boldsymbol{p}_{T2}, -\boldsymbol{p}_{T1}, -\boldsymbol{p}_{T2}). \tag{21}$$

Therefore, from this kinematic region the correlations are determined by the impact factor. Using the impact factor given in Eq. (15), we see that

$$I_P(\boldsymbol{p}_{T1}, \boldsymbol{p}_{T2}, \boldsymbol{p}_{T1}, \boldsymbol{p}_{T2}) = 2 + F(2(\boldsymbol{p}_{T1} + \boldsymbol{p}_{T2})) + F(2\boldsymbol{p}_{T,12}) - 2F(2\boldsymbol{p}_{T1}) - 2F(\boldsymbol{p}_{T2}). \tag{22}$$

This function is symmetric with respect to $\phi \to \pi - \phi$ ($\boldsymbol{p}_{T1} \to -\boldsymbol{p}_{T1}$), and with such an impact factor the Born approximation produces only $v_n$ with even $n$, as was noted in Ref. [2,3]. However, this conclusion is based on the impact factor of Eq. (15). Equation (22) shows that this impact factor leads to $p_{T,12} \sim 1/R_N$.

Note that the simple expression of Eq. (15) (see Fig. 4) is written for sufficiently hard gluons. For small values of $Q_T = p_{T,12}$, we need to add the first diagram of Fig. 5, in which there are two gluons with large transverse momenta (about $p_{T1}$ or $p_{T2}$) but small $Q_T$. The final expression for the impact factor takes the form

$$I_P^F(\boldsymbol{k}_T, \boldsymbol{l}_T, -\boldsymbol{l}_T + \boldsymbol{Q}_T, -\boldsymbol{k}_T + \boldsymbol{Q}_T) = I_P(\boldsymbol{k}_T, -\boldsymbol{k}_T + \boldsymbol{Q}_T) I_P(\boldsymbol{l}_T, -\boldsymbol{l}_T - \boldsymbol{Q}_T) + \underbrace{I_P(\boldsymbol{k}_T, \boldsymbol{l}_T, -\boldsymbol{l}_T + \boldsymbol{Q}_T, -\boldsymbol{k}_T + \boldsymbol{Q}_T)}_{\text{Eq. (15)}}. \tag{23}$$

The first term in Eq. (23) generates a correlation function which is proportional to $F^2(2\boldsymbol{p}_{T,12})$.

Summarizing, we see that the Born approximation of perturbative QCD generates a correlation function which is determined by the impact factor of the nucleon, that the typical correlation length is about $R_N$, and that, even for the unrealistic perturbative model of onium, this correlation function is not symmetric with respect to $\phi \to \pi - \phi$. We will consider the more realistic case below in the leading log approximation (LLA) of perturbative QCD. However, we would like to stress now that the correlation function stems from the large nonperturbative distances of the order of the nucleon size.

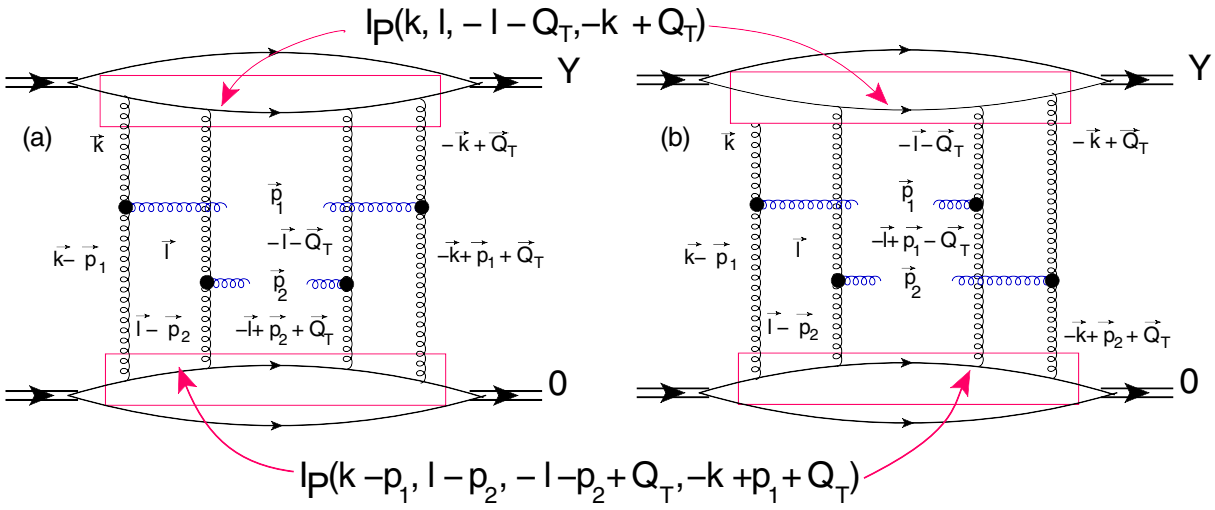


FIG. 6. The double inclusive production of two gluons with rapidities $y_1$ and $y_2$ and transverse momenta $\boldsymbol{p}_{T1}$ and $\boldsymbol{p}_{T2}$ in the Born Approximation of perturbative QCD for the nucleon-nucleon interaction. Figure 6(a) corresponds to the square of the diagrams of Fig. 1. The interference diagram of Fig. 6(b) yields the correlation function $C(R_D|\boldsymbol{p}_{T1} - \boldsymbol{p}_{T2}|)$ of Eq. (2). The solid lines denote nucleons in the deuterons, which are illustrated by double lines.

### C. Bose-Einstein correlation function with radius $\propto R_N$: Nucleon-nucleon interaction

The correlations with $R_c = R_N$ are typical for nucleon-nucleon interaction (see Fig. 6 for the Born approximation of perturbative QCD). However, we will consider them below for the general case of the production of two-parton showers since we prefer to use a more phenomenological and realistic approach for the impact factors $I_P$ than we explored above, replacing the nucleon with the onium state.

## III. PRODUCTION OF TWO-PARTON SHOWERS

### A. $R_c \propto R_D$

In this section we consider the general case of the production of two-parton showers shown in Fig. 1. In the leading log approximation of perturbative QCD, the structure of a one-parton shower is described by the Balitski-Fadin-Kuraev-Lipatov (BFKL) Pomeron [22,23]. In the leading log approximation of perturbative QCD the Born diagram of Fig. 2(a) can be generalized to Fig. 7. The contribution of this diagram can be written as follows:

$$\frac{d^2\sigma}{dy_1 dy_2 d^2p_{T1} d^2p_{T2}}(\text{Fig.7}) = \left(\frac{2\pi\bar{\alpha}_S}{C_F}\right)^2 \frac{1}{p^2_{T,1}p^2_{T2}} \int d^2Q_T G^2_D(Q_T) \times \left(\int d^2k_T \phi^N_G(Y-y_1;\boldsymbol{k}_T,-\boldsymbol{k}_T+\boldsymbol{Q}_T)\phi^N_G(y_1;\boldsymbol{k}_T-\boldsymbol{p}_{T1},-\boldsymbol{k}_T+\boldsymbol{p}_{T1}+\boldsymbol{Q}_T)\right) \times \left(\int d^2l_T \phi^N_G(Y-y_2;\boldsymbol{l}_T,-\boldsymbol{l}_T-\boldsymbol{Q}_T)\phi^N_G(y_2;\boldsymbol{l}_T-\boldsymbol{p}_{T2},-\boldsymbol{l}_T+\boldsymbol{p}_{T2}-\boldsymbol{Q}_T)\right), \tag{24}$$

where $\phi^N_G(y,\boldsymbol{k}_T,-\boldsymbol{k}_T+\boldsymbol{Q}_T)$ denotes the probability to find a gluon with rapidity $y$ and transverse momentum $k_\perp$, in the process with momentum transferred $Q_T$. In Eq. (24) $\bar{\alpha}_S = \alpha_S N_c/\pi$ with the number of colors equal to $N_c$. $\phi^N_G$ are the solutions of the BFKL evolution equation

$$\frac{\partial\phi^N_G(y,\boldsymbol{k}_T,-\boldsymbol{k}_T+\boldsymbol{Q}_T)}{\partial y} = \bar{\alpha}_S \int \frac{d^2k'_T}{2\pi} K(Q_T;k_T,k'_T)\phi^N_G(y,\boldsymbol{k}'_T,-\boldsymbol{k}'_T+\boldsymbol{Q}_T) - (\omega_G(\boldsymbol{Q}_T-\boldsymbol{k}_T)+\omega_G(\boldsymbol{k}_T))\phi^N_G(y,\boldsymbol{k}_T,-\boldsymbol{k}_T+\boldsymbol{Q}_T), \tag{25}$$

where

$$K(Q_T,k_T,k'_T) = \frac{1}{(\boldsymbol{k}_T-\boldsymbol{k}'_T)^2}\left\{\frac{k^2_T}{k'^2_T} + \frac{(\boldsymbol{Q}_T-\boldsymbol{k}_T)^2}{(\boldsymbol{Q}_T-\boldsymbol{k}'_T)^2} - \frac{(\boldsymbol{k}_T-\boldsymbol{k}'_T)^2}{k'^2_T(\boldsymbol{Q}_T-\boldsymbol{k}'_T)^2}\right\}$$
$$\omega_G(\boldsymbol{k}_T) = \frac{1}{2}\bar{\alpha}_S k^2_T \int \frac{d^2k'_T}{2\pi}\frac{1}{k'^2_T(\boldsymbol{k}_T-\boldsymbol{k}'_T)^2}. \tag{26}$$

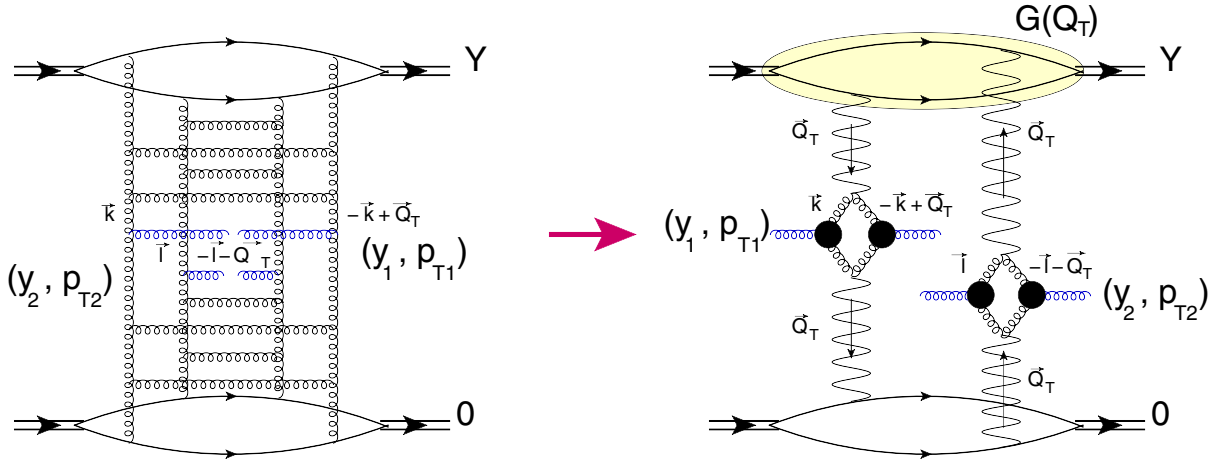


FIG. 7. The double inclusive production of two gluons with rapidities $y_1$ and $y_2$ and transverse momenta $\boldsymbol{p}_{T1}$ and $\boldsymbol{p}_{T2}$ for the exchange of two BFKL Pomerons which are denoted by wavy lines. This diagram is the LLA generalization of Fig. 2(a). The solid lines denote nucleons in the deuterons, which are indicated by double lines.

The typical momenta in $\phi^N_G$ are about $1/R_N$ or larger, (about $p_{T1}$ ($p_{T2}$), or $Q_s$, where $Q_s$ denotes the saturation scale. Bearing this in mind, and noting that $Q_T \sim 1/R_D \ll 1/R_N$, we can put $Q_T = 0$ in the arguments of $\phi^N_G$. This simplifies Eq. (24), reducing it to the following expression:

$$\frac{d^2\sigma}{dy_1 dy_2 d^2p_{T1} d^2p_{T2}}(\text{Fig.7}) = \frac{d^2\sigma}{dy_1 d^2p_{T1}} \frac{d^2\sigma}{dy_2 d^2p_{T2}} \times \int d^2Q_T G^2_D(Q_T). \tag{27}$$

The diagram of Fig. 2(b) in the LLA simplifies the expression for the exchange of two BFKL Pomerons, but with more complicated vertices. Using Eq. (10) and considering $\bar{\alpha}_S(y_1 - y_2) \leq 1$, we can write this exchange in the form that is represented in Fig. 8, and its contribution has the following form:

$$\begin{aligned}
&\frac{d^2\sigma}{dy_1 dy_2 d^2p_{T1} d^2p_{T2}}(\text{Fig.8}) \\
&= \frac{1}{2}\left(\frac{2\pi\bar{\alpha}_S}{C_F}\right)^2 \int d^2Q_T G_D(Q_T) G_D(\boldsymbol{Q}_T - \boldsymbol{p}_{T,12}) \\
&\times \left(\int d^2k_T \phi^N_G(Y - y_1; \boldsymbol{k}_T, -\boldsymbol{k}_T + \boldsymbol{Q}_T) \Gamma_\mu(k_T, p_{T1}) \Gamma_\mu(-\boldsymbol{k}_T + \boldsymbol{Q}_T, p_{T2}) \phi^N_G(y_2; \boldsymbol{k}_T - \boldsymbol{p}_{T1}, -\boldsymbol{k}_T + \boldsymbol{p}_{T2} + \boldsymbol{Q}_T)\right) \\
&\times \left(\int d^2l_T \phi^N_G(Y - y_1; \boldsymbol{l}_T, -\boldsymbol{l}_T - \boldsymbol{Q}_T) \Gamma_\mu(l_T, p_{T1}) \Gamma_\mu(-\boldsymbol{l}_T - \boldsymbol{Q}_T, p_{T2}) \phi^N_G(y_2; \boldsymbol{l}_T - \boldsymbol{p}_{T2}, -\boldsymbol{l}_T + \boldsymbol{p}_{T1} - \boldsymbol{Q}_T)\right).
\end{aligned} \tag{28}$$

Since $Q_T \sim 1/R_B \ll 1/R_N$ as well as $|\boldsymbol{Q}_T - \boldsymbol{p}_{T,12}| \sim 1/R_D \ll 1/R_N$, we can take both $Q_T = 0$ and $p_{T,12} = 0$, but it is not sufficient to reduce Eq. (28) to Eq. (12). In addition, we need to assume that $\bar{\alpha}_S(y_1 - y_2) \leq 1$. Making this assumption, we can replace $y_2$ in $\phi^N_G(y_2; \boldsymbol{k}_T - \boldsymbol{p}_{T1}, -\boldsymbol{k}_T + \boldsymbol{p}_{T2} + \boldsymbol{Q}_T)$ with $y_1$, and $Y - y_1$ in $\phi^N_G(Y - y_1; \boldsymbol{l}_T, -\boldsymbol{l}_T - \boldsymbol{Q}_T)$ with $Y - y_2$. After these changes, Eq. (28) can be reduced to the following expression:

$$\begin{aligned}
&\frac{d^2\sigma}{dy_1 dy_2 d^2p_{T1} d^2p_{T2}}(\text{Fig.8}) \\
&= \frac{d^2\sigma}{dy_1 d^2p_{T1}} \frac{d^2\sigma}{dy_2 d^2p_{T2}} \int d^2Q_T G_D(Q_T) G_D(\boldsymbol{Q}_T + \boldsymbol{p}_{T,12}).
\end{aligned} \tag{29}$$

Eq. (27) and Eq. (29) lead to the same correlation function $[C(R_D p_{T,12})]$ Eq. (12) as in the Born approximation.

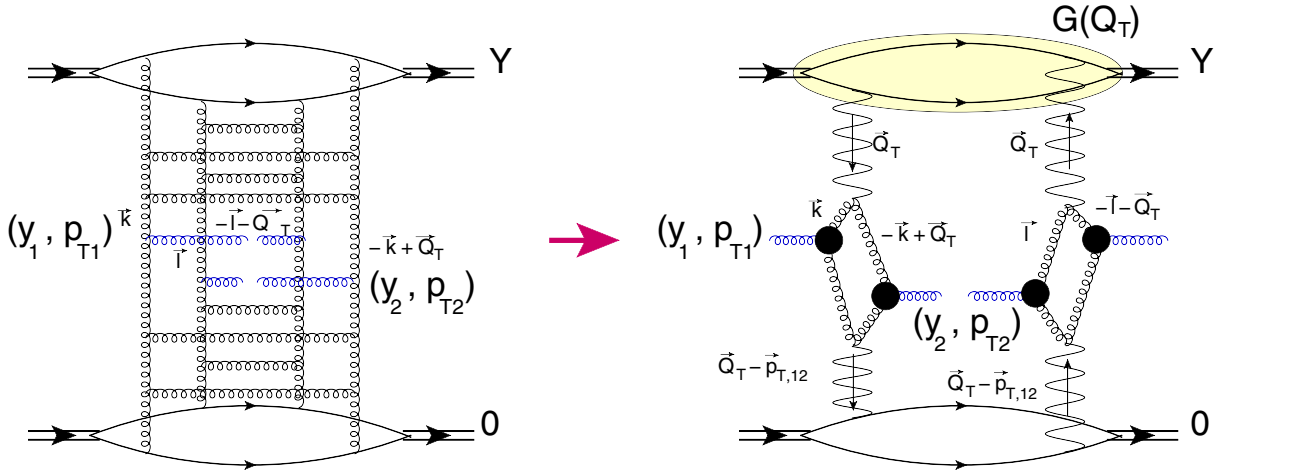


FIG. 8. The double inclusive production of two gluons with rapidities $y_1$ and $y_2$ and transverse momenta $\boldsymbol{p}_{T1}$ and $\boldsymbol{p}_{T2}$ for the exchange of two BFKL Pomerons, which are denoted by wavy lines. This diagram is the LLA generalization of Fig. 2(b). The solid lines denote nucleons in the deuterons, which are represented by double lines.

### B. $R_c \propto R_N$

In LLA the diagrams of the Born approximation of Fig. 3 can be generalized in the same way as has been discussed above. Figure 3(a) takes the form of Fig. 9, while the interference diagram of Fig. 3(b) becomes Fig. 10.

The contribution of the diagram of Fig. 9 can be written as follows:

$$\frac{d^2\sigma}{dy_1 dy_2 d^2p_{T1} d^2p_{T2}}(\text{Fig.9}) = \left(\frac{2\pi\bar{\alpha}_S}{C_F}\right)^2 \frac{1}{p_{T,1}^2 p_{T2}^2} \int d^2Q_T N(Q_T) G_D^2(Q_T)$$
$$\times \left(\int d^2k_T \phi_G^N(Y-y_1;\boldsymbol{k}_T,-\boldsymbol{k}_T+\boldsymbol{Q}_T)\phi_G^N(y_1;\boldsymbol{k}_T-\boldsymbol{p}_{T1},-\boldsymbol{k}_T+\boldsymbol{p}_{T1}+\boldsymbol{Q}_T)\right)$$
$$\times \left(\int d^2l_T \phi_G^N(Y-y_2;\boldsymbol{l}_T,-\boldsymbol{l}_T-\boldsymbol{Q}_T)\phi_G^N(y_2;\boldsymbol{l}_T-\boldsymbol{p}_{T2},-\boldsymbol{l}_T+\boldsymbol{p}_{T2}-\boldsymbol{Q}_T)\right), \quad (30)$$

where $N(Q_T)$ denotes the integral over all energies of the imaginary part of the Pomeron-nucleon scattering amplitude. This amplitude was introduced in Gribov's Pomeron calculus [25], but it has been proven that we can use this formalism in LLA of perturbative QCD [26]. $N(Q_T)$ has the following general form (see Fig. 11):

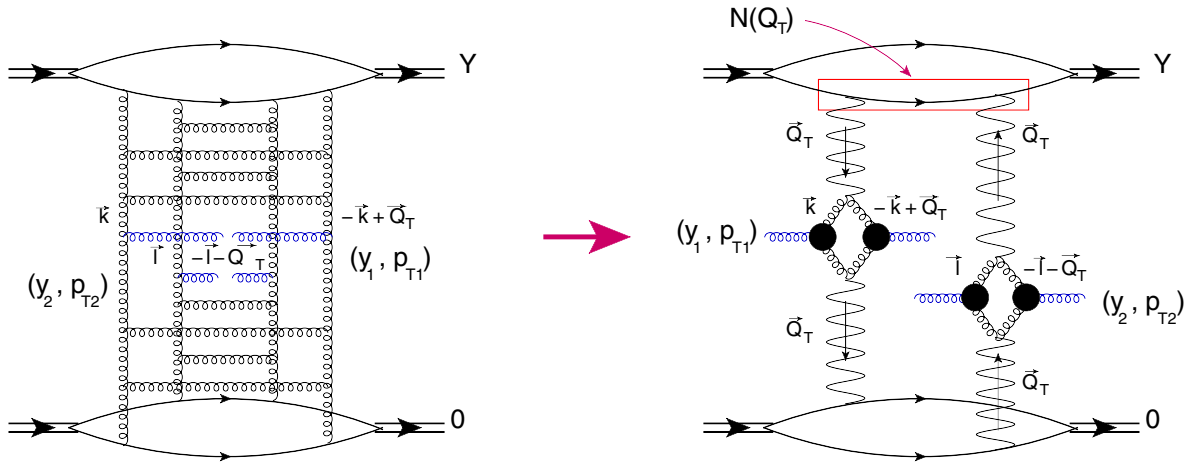


FIG. 9. The Mueller diagram [24] for the double inclusive production of two gluons with rapidities $y_1$ and $y_2$ and transverse momenta $\boldsymbol{p}_{T1}$ and $\boldsymbol{p}_{T2}$ for the exchange of two BFKL Pomerons, which are denoted by wavy lines. This diagram is the LLA generalization of Fig. 3(a). The solid lines denote nucleons in the deuterons, which are illustrated by double lines.

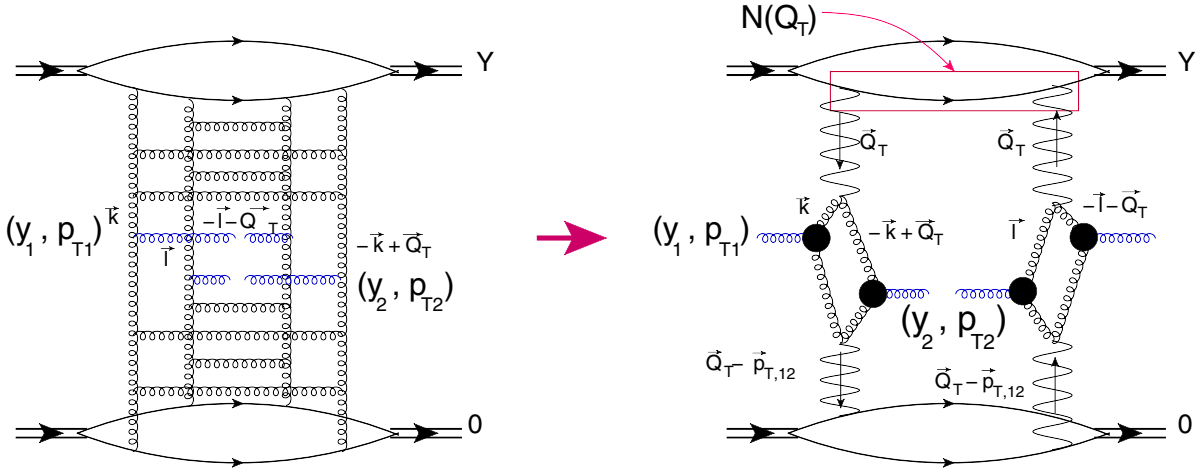


FIG. 10. The Mueller diagram for the double inclusive production of two gluons with rapidities $y_1$ and $y_2$ and transverse momenta $\boldsymbol{p}_{T1}$ and $\boldsymbol{p}_{T2}$ for the exchange of two BFKL Pomerons, which are denoted by wavy lines. This diagram is the LLA generalization of Fig. 3(b). The solid lines denote nucleons in the deuterons, which are illustrated by double lines.

$$N(Q_T) = \underbrace{g^2(Q_T)}_{\text{elastic scattering}} + \underbrace{\sum_{M_i=m}^{M_0} g^2(Q_T;M_i)}_{\text{diffraction in low masses}} + \underbrace{\int_{M_0} \frac{dM^2}{M^2}\phi^N_G(y_M, Q_T=0;\{\ldots\})G_{3\mathbb{P}}(Q_T,\{\ldots\})}_{\text{diffraction in high masses}}, \tag{31}$$

where $G_{3\mathbb{P}}$ is the triple BFKL Pomeron vertex, and $\{\ldots\}$ denotes all transverse momenta which we need to integrate over. $y_M = \ln(M^2/M_0^2)$.

Figure 11(b) shows how all contributions correspond to the onium case, where we can use perturbative QCD for theoretical estimates.

Since $Q_T \sim 1/R_D \ll 1.R_N$, and all other transverse momenta in Fig. 9 are either of the order of $1/R_N$ or larger (of the order of $p_{T1}$,$p_{T2}$ or $Q_s$, where $Q_s$ is the saturation scale), we can safely put $Q_T = 0$ and reduce this contribution to the factorized form

$$\frac{d^2\sigma}{dy_1 dy_2 d^2p_{T1} d^2p_{T2}}(\text{Fig.9}) = \frac{d^2\sigma}{dy_1 d^2p_{T1}}\frac{d^2\sigma}{dy_2 d^2p_{T2}} N(Q_T=0)\int d^2Q_T G_D(Q_T). \tag{32}$$

The contribution of the relevant diagram, which is shown in Fig. 10, can be written in the form

$$\begin{aligned}
&\frac{d^2\sigma}{dy_1 dy_2 d^2p_{T1} d^2p_{T2}}(\text{Fig.10})\\
&= \frac{1}{2}\left(\frac{2\pi\bar{\alpha}_S}{C_F}\right)^2 \int d^2Q_T N(Q_T) G_D(\boldsymbol{Q}_T - \boldsymbol{p}_{T,12})\\
&\times \left(\int d^2k_T \phi^N_G(Y-y_1;\boldsymbol{k}_T, -\boldsymbol{k}_T+\boldsymbol{Q}_T)\Gamma_\mu(k_T,p_{T1})\Gamma_\mu(-\boldsymbol{k}_T+\boldsymbol{Q}_T,p_{T2})\phi^N_G(y_2;\boldsymbol{k}_T-\boldsymbol{p}_{T1},-\boldsymbol{k}_T+\boldsymbol{p}_{T2}+\boldsymbol{Q}_T)\right)\\
&\times \left(\int d^2l_T \phi^N_G(Y-y_1;\boldsymbol{l}_T, -\boldsymbol{l}_T-\boldsymbol{Q}_T)\Gamma_\mu(l_T,p_{T1})\Gamma_\mu(-\boldsymbol{l}_T-\boldsymbol{Q}_T,p_{T2})\phi^N_G(y_2;\boldsymbol{l}_T-\boldsymbol{p}_{T2},-\boldsymbol{l}_T+\boldsymbol{p}_{T1}-\boldsymbol{Q}_T)\right).
\end{aligned} \tag{33}$$

Integration over $Q_T$ leads to $\boldsymbol{Q}_T - \boldsymbol{p}_{T,12} \sim 1/R_D \ll 1/R_N$; therefore, as in the Born approximation, we can put $\boldsymbol{Q}_T = \boldsymbol{p}_{T,12}$. In Eq. (33) we have two sources of $p_{T,12}$ behavior: $N(p_{T,12})$ and $\phi^N_G$. Replacing $\boldsymbol{Q}_T = \boldsymbol{p}_{T,12}$, we obtain

$$\begin{aligned}
&\frac{d^2\sigma}{dy_1 dy_2 d^2p_{T1} d^2p_{T2}}(\text{Fig.10})\\
&= \frac{1}{2}\left(\frac{2\pi\bar{\alpha}_S}{C_F}\right)^2 \int d^2Q_T N(p_{T,12}) G_D(\boldsymbol{Q}_T - \boldsymbol{p}_{T,12})\\
&\times \left(\int d^2k_T \phi^N_G(Y-y_1;\boldsymbol{k}_T, -\boldsymbol{k}_T+\boldsymbol{p}_{T,12})\frac{1}{k_T^2(\boldsymbol{k}_T-\boldsymbol{p}_{T,12})^2(\boldsymbol{k}_T-\boldsymbol{p}_{T,1})^4}\phi^N_G(y_2;\boldsymbol{k}_T-\boldsymbol{p}_{T1},-\boldsymbol{k}_T+\boldsymbol{p}_{T1})\right.\\
&\left.\times\left\{\frac{(\boldsymbol{k}_T-\boldsymbol{p}_{T,12})^2(\boldsymbol{k}_T-\boldsymbol{p}_{T,1})^2}{p^2_{T2}} + \frac{k_T^2(\boldsymbol{k}_T-\boldsymbol{p}_{T,1}-\boldsymbol{p}_{T,12})^2}{p^1_{T2}} - p^2_{T,12} - p^2_{T,12}\frac{k_T^2(\boldsymbol{k}_T-\boldsymbol{p}_{T,12})^2}{p^1_{T2}p^2_{T,2}}\right\}\right)\\
&\times \left(\int d^2l_T \phi^N_G(Y-y_1;\boldsymbol{l}_T, -\boldsymbol{l}_T-\boldsymbol{p}_{T,12})\frac{1}{l_T^2(\boldsymbol{l}_T+\boldsymbol{p}_{T,12})^2(\boldsymbol{l}_T-\boldsymbol{p}_{T,2})^4}\phi^N_G(y_2;\boldsymbol{l}_T-\boldsymbol{p}_{T2},-\boldsymbol{l}_T+\boldsymbol{p}_{T2})\right.\\
&\left.\times\left\{\frac{(\boldsymbol{l}_T+\boldsymbol{p}_{T,12})^2(\boldsymbol{l}_T-\boldsymbol{p}_{T,1})^2}{p^2_{T2}} + \frac{l_T^2(\boldsymbol{l}_T-\boldsymbol{p}_{T,2})^2}{p^1_{T2}} - p^2_{T,12} - p^2_{T,12}\frac{l_T^2(\boldsymbol{l}_T+\boldsymbol{p}_{T,12})^2}{p^1_{T2}p^2_{T,2}}\right\}\right).
\end{aligned} \tag{34}$$

The products of $G_\mu G_\mu$ are written in Eq. (34) $\{\ldots\}$ explicitly using Eq. (6), and $\phi^N_D$ is the solution of Eq. (25). Recall that $\phi^N_D(\boldsymbol{k}_T, -\boldsymbol{k}_T+\boldsymbol{Q}_T)$ vanishes both at $k_T \to 0$ and $\boldsymbol{k}_T - \boldsymbol{Q}_T \to 0$. Since the products of $G_\mu$ vanish at $\boldsymbol{k}_T - \boldsymbol{p}_{T1} \to 0$ or $\boldsymbol{l}_T - \boldsymbol{p}_{T2} \to 0$, respectively, we can conclude that the integrals over $k_T$ and $l_T$ do not have large contributions at $k_T$ of the order of $p_{T1}$ and at $l_T$ of the order of $p_{T2}$.

In the appendix we show that the typical value of $Q_T$ for the BFKL Pomeron $\phi^N_G(Y;k'_T,k_T,Q_T)$ is determined by the smallest value of transverse momentum $Q_T \sim min\{k;_T, k_T\}$. In our case this means that $Q_T = p_{T,12} \sim 1/R_N \gg p_{T1}$ and/or $p_{T2}$.

Therefore, we can rewrite Eq. (34) as follows:

$$\frac{d^2\sigma}{dy_1 dy_2 d^2p_{T1} d^2p_{T2}}(\text{Fig.10}) = \frac{1}{2}\left(\frac{2\pi\bar{\alpha}_S}{C_F}\right)^2 \frac{1}{p_{T1}^2 p_{T2}^2}\int d^2Q_T N(p_{T,12}) G_D(\boldsymbol{Q}_T - \boldsymbol{p}_{T,12}) \times \left(\int d^2k_T \phi_G^N(Y-y_1;\boldsymbol{k}_T,-\boldsymbol{k}_T)\phi_G^N(y_2;\boldsymbol{k}_T-\boldsymbol{p}_{T1},-\boldsymbol{k}_T+\boldsymbol{p}_{T1})\right) \times \left(\int d^2l_T \phi_G^N(Y-y_1;\boldsymbol{l}_T,-\boldsymbol{l}_T)\phi_G^N(y_2;\boldsymbol{l}_T-\boldsymbol{p}_{T2},-\boldsymbol{l}_T+\boldsymbol{p}_{T2})\right). \quad (35)$$

In Eq. (35) we introduce $\phi_G^N(\boldsymbol{k}_t,-\boldsymbol{k}_T) = (1/k_T^2)\phi_G^N(\boldsymbol{k}_t,-\boldsymbol{k}_T)$ [Eq. (34)]. Comparing Eq. (32) and Eq. (35), one can see that the correlation function is equal to

$$C(R_N^2 p_{T,12}^2) = N(p_{12}^2) \quad (36)$$

for $\bar{\alpha}_S(y_1 - y_2) \le 1$.

The three terms of $N(Q_T)$ are shown in Fig. 11(a). The first contribution $N(Q_T) = g^2(Q_T)$ can easily be evaluated from the differential elastic cross section, which is proportional to $g^4(Q_T)$. Recall that the BFKL Pomeron does not generate the shrinkage of the diffraction peak seen in the experimental data. This indicates that the exchange of the single BFKL Pomeron is not sufficient to describe the high-energy amplitude, and we need to use a more phenomenological approach to describe the elastic contribution to the correlation function (see Ref. [4], in which we tried to describe these correlations using a particular model for high-energy scattering, which is based on CGC/saturation approach).

For the onium, $g(Q_T)$ can be calculated [see Fig. 11(b) and Eq. (B5)] in the following way:

$$g(Q_T) = V^{\text{onium}}(\boldsymbol{Q}_T) = \int d^2k'_T I_P(\boldsymbol{k}_T,-\boldsymbol{k'}_T+\boldsymbol{Q}_T)V^{\text{pr}}(\boldsymbol{k'}_T,\boldsymbol{Q}_T) = \int d^2k'_T (F(Q_T) - F(2\boldsymbol{k'}_T - \boldsymbol{Q}_T))V^{\text{pr}}_{\frac{1}{2}}(\boldsymbol{k'_T},\boldsymbol{Q}_T), \quad (37)$$

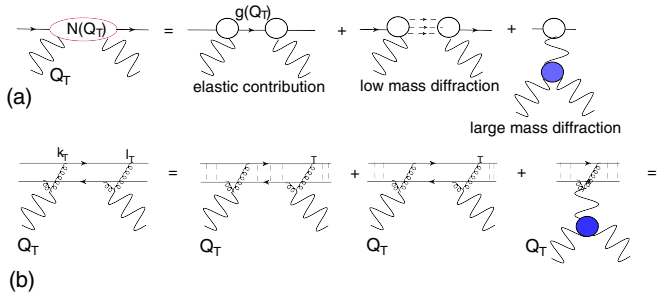


FIG. 11. The structure of the amplitude $N(Q_T)$. Figure 11(a) shows the BFKL Pomeron-nucleon interaction, and Fig. 11(b) shows the BFKL Pomeron-onium interactions. The blob shows the triple BFKL Pomeron vertex which is the same for both figures. The dashed vertical lines describe the Coulomb gluons that create the bound state: onium.

where $V^{\text{pr}}$ is determined by Eq. (B4). In Eq. (37) $k'_T \sim 1/R_N \ll k_T$. Assuming that $F(Q_T)$ of Eq. (15) is equal to $1/(1+R_N^2Q_T^2)$, we find that at large $Q_T$, $g(R_N Q_T)$ decreases as $1/Q_T$.

The second term of Fig. 11(b) can be evaluated from the process of diffraction dissociation in the region of small masses. However, we need to use a model for this term to be able to extract its $Q_T$ dependence from the experimental data. For example, we can replace the sum of possible produced diffractive states with one state, as has been done in Ref. [4]. For the onium state, this term has the following form:

$$N_{\text{diff}}(Q_T) = \int d^2k'_T \int d^2l'_T I_P(\boldsymbol{k}_T,\boldsymbol{l}_T,-\boldsymbol{l}_T+\boldsymbol{Q}_T,-\boldsymbol{k}_T+\boldsymbol{Q}_T) \times V^{\text{pr}}(\boldsymbol{k'}_T;\boldsymbol{Q}_T)V^{\text{pr}}(\boldsymbol{l'}_T;\boldsymbol{Q}_T), \quad (38)$$

where $I_P$ is taken from Eq. (15).

Using Eq. (B4) we calculate $N_{\text{diff}}(Q_T)$ which decreases as $1/Q_T^2$ at large $Q_T$.

### C. $R_c \propto 1/Q_s$

The last term in Fig. 11(a) gives the contribution of large mass production in the diffraction dissociation process. The $Q_T$ dependence of this term is determined by the triple BFKL Pomeron vertex in perturbative QCD (see Fig. 12). Therefore, this term generates correlations, whose length is

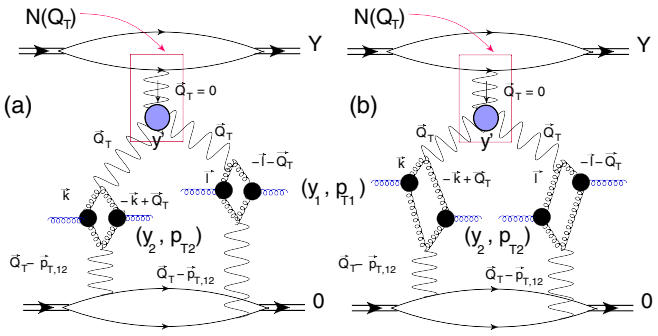


FIG. 12. The large mass diffraction contribution to $N(Q_T)$, the source for the correlation length of about $1/Q_s$. The blue blob denotes the triple BFKL Pomeron vertex. The red square indicates the contribution of $N(Q_T)$, which includes the integration over rapidity $y'$. Figure 12(a) corresponds to the square of the diagrams of Fig. 1. Figure 12(b) describes the interference term of these diagrams.

determined by the BFKL Pomeron structure, and it is closely related to the typical saturation momentum $Q_s$.

Comparing Fig. 12 with Fig. 9 and Fig. 10, one can see that the difference is only in the expression for $N(Q_T)$, which has the following form

$$N_{\text{large mass diffraction}}(Q_T) = \int dy' \phi_G^N(Y-y';Q_T=0;q_T,q'_T) \times d^2q'_T G_{3\mathbb{P}}(q'_T;k'_T,l'_T,Q_T). \quad (39)$$

We can obtain the form of $G_{3\mathbb{P}}$ in momentum space starting from the coordinate representation, where the contribution of the triple Pomeron diagram of Fig. 13 is known [27,28], as follows:

$$\bar{\alpha}_S \int \frac{d^2x_0 d^2x_1 d^2x_2}{x_{01}^2 x_{02}^2 x_{21}^2} N(x'_{01},x_{01};\boldsymbol{b}-\boldsymbol{b}';Y-y') \times N\left(x'_{02},x_{02};\boldsymbol{b}'-\frac{1}{2}\boldsymbol{x}_{21};y'-y_1\right) \times N\left(x'_{21},x_{21};\boldsymbol{b}'-\frac{1}{2}\boldsymbol{x}_{02};y'-y_2\right). \quad (40)$$

Introducing [18]

$$N(x_{01},b;Y) = x_{01}^2 \int d^2k d^2Q_T e^{i\boldsymbol{k}_T\cdot\boldsymbol{x}_{01}+i\boldsymbol{Q}_T\cdot\boldsymbol{b}} N(k_T,Q_T), \quad (41)$$

we see that Eq. (41) can be rewritten in the form

$$\bar{\alpha}_S \int d^2q'_T N(q_T,q'_T,Q_T=0,Y-y') \times G_{3\mathbb{P}}(q'_T;k'_T,l'_T,Q_T) N(k'_T,k_T,Q_T,y'-y_1) \times N(l'_T,l_T,-Q_T,y'-y_2), \quad (42)$$

with

$$G_{3\mathbb{P}}(q'_T;k'_T,l'_T,Q_T) = \delta^{(2)}\left(\boldsymbol{k'}_T-\boldsymbol{q}'+\frac{1}{2}\boldsymbol{Q}_T\right) \times \delta^{(2)}\left(\boldsymbol{l'}_T-\boldsymbol{q}'-\frac{1}{2}\boldsymbol{Q}_T\right). \quad (43)$$

In Eq. (39) we use the following notation for $\phi_G^N(Y-y';Q_T=0;k_i,k_f)$: $Y-y'$ is the rapidity, $Q_T$ is the momentum transfer of the BFKL Pomeron, $k_i$ and $k_f$ are initial and final transverse momenta. Plugging Eq. (43) into the general expression for the interference diagram of Fig. 12(b), we see that instead of Eq. (34) we obtain

$$\frac{d^2\sigma}{dy_1 dy_2 d^2p_{T1} d^2p_{T2}}(\text{Fig.12}-\text{b}) = \frac{1}{2}\left(\frac{2\pi\bar{\alpha}_S}{C_F}\right)^2 \int d^2Q_T G_D(\boldsymbol{Q}_T-\boldsymbol{p}_{T,12}) \int dy' \int \phi_G^N(Y-y';Q_T=0;q_T,q'_T) d^2q'_T \times \left( G^{\text{BFKL}}\left(y'-y_1;p_{T,12};\boldsymbol{q'}_T-\frac{1}{2}\boldsymbol{p}_{T,12},k_T\right)\frac{1}{k_T^2(\boldsymbol{k}_T-\boldsymbol{p}_{T,12})^2(\boldsymbol{k}_T-\boldsymbol{p}_{T,1})^4} G^{\text{BFKL}}(y_2;0;\boldsymbol{k}_T-\boldsymbol{p}_{T1},k_N) \times \left\{\frac{(\boldsymbol{k}_T-\boldsymbol{p}_{T,12})^2(\boldsymbol{k}_T-\boldsymbol{p}_{T,1})^2}{p_{T2}^2}+\frac{k_T^2(\boldsymbol{k}_T-\boldsymbol{p}_{T,1}-\boldsymbol{p}_{T,12})^2}{p_{T2}^1}-p_{T,12}^2-p_{T,12}^2\frac{k_T^2(\boldsymbol{k}_T-\boldsymbol{p}_{T,12})^2}{p_{T2}^1 p_{T,2}^2}\right\}\right) \times \left( \int d^2l_T G^{\text{BFKL}}\left(y'-y_1;p_{T,12},\boldsymbol{q'}_T+\frac{1}{2}\boldsymbol{p}_{T,12},l_T\right)\frac{1}{l_T^2(\boldsymbol{l}_T+\boldsymbol{p}_{T,12})^2(\boldsymbol{l}_T-\boldsymbol{p}_{T,2})^4} G^{\text{BFKL}}(y_2;0;\boldsymbol{l}_T-\boldsymbol{p}_{T2},l_N) \times \left\{\frac{(\boldsymbol{l}_T+\boldsymbol{p}_{T,12})^2(\boldsymbol{l}_T-\boldsymbol{p}_{T,1})^2}{p_{T2}^2}+\frac{l_T^2(\boldsymbol{l}_T-\boldsymbol{p}_{T,2})^2}{p_{T2}^1}-p_{T,12}^2-p_{T,12}^2\frac{l_T^2(\boldsymbol{l}_T+\boldsymbol{p}_{T,12})^2}{p_{T2}^1 p_{T,2}^2}\right\}\right). \quad (44)$$

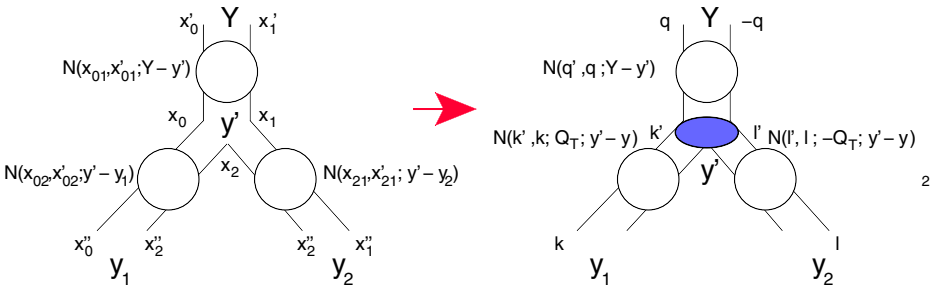


FIG. 13. The triple BFKL Pomeron vertex in coordinate and momentum representations. The blue blob denotes the triple Pomeron vertex.

The main difference between Eq. (44) and Eq. (34) is that $q'_T$ is larger than $q_T \approx 1/R_N$. Indeed, the typical value of $q'_T = Q_s(Y-y') \sim (1/R_N^2)\exp(\lambda(Y-y'))$, where $\lambda = \omega(\gamma_{cr},0)/(1-\gamma_{cr})$ with $\gamma_{cr}=0.37$ in leading order of perturbative QCD [18].

From Eq. (A16) one can see that each $\phi_D^N(Y-y') \propto e^{\omega(\frac{1}{2},0)(Y-y')}$, $\phi_D^N(y'-y_1) \propto e^{\omega(\frac{1}{2},0)(y'-y_1)}$, and $\phi_D^N(y'-y_2) \propto e^{\omega(\frac{1}{2},0)(y'-y_2)}$ since $\gamma = \frac{1}{2}+i\nu$ with small $\nu$. Therefore, integration over $y'$ results in $Y-y' \sim 1/\omega(\frac{1}{2},0) \propto 1/\bar{\alpha}_S$, while $y'-y_1$ and $y'-y_2$ are large (of the order of $Y$). Since $Y-y' \ll y'-y_1$ ($Y-y' \ll y'-y_2$), we can use the factorized formula of Eq. (A15) for $\phi_G^N(y'-y_1; p_{T,12}; \boldsymbol{q}'_T - \frac{1}{2}\boldsymbol{p}_{T,12}, k_T)$ and for $\phi_G^N(y'-y_1; p_{T,12}, \boldsymbol{q}'_T + \frac{1}{2}\boldsymbol{p}_{T,12}, l_T)$. Using Eq. (A15) we find that $p_{T,12}$ will be determined by the lowest momenta in the BFKL Pomeron with $y'-y_1$, and it will have the form

$$C(p_{T,12}) \propto \int d^2q'_T I_{-\gamma}(q'_T) V_\gamma\left(\boldsymbol{q}'_T - \frac{1}{2}\boldsymbol{Q}_T, \boldsymbol{Q}_T\right) \times V_\gamma\left(\boldsymbol{q}'_T + \frac{1}{2}\boldsymbol{Q}_T, \boldsymbol{Q}_T\right), \tag{45}$$

where $V$ is determined by Eq. (A12), and $Q_T = p_{T,12}$. In Eq. (45) we can put $\gamma = \frac{1}{2}$, assuming $y'-y_1$ is sufficiently large that we can neglect $\nu$.

## IV. BOSE-EINSTEIN CORRELATION FUNCTION IN THE NUCLEON-NUCLEON INTERACTION

In this section we discuss the Bose-Einstein correlations in nucleon-nucleon scattering. The Mueller diagrams for the square of the diagrams Fig. 1(a) and Fig. 1(b), and for the interference diagrams, are shown in Fig. 14. This differs from the diagrams that have been discussed above only in the appearance of the second $N(Q_T)$, which reflects the fact that we do not have small (about $1/R_D$) momenta in this process. Note that we can use perturbative QCD only if $p_{T1} \sim p_{T2} \gg 1/R_N$. Recalling that the $Q_T$ dependence of the BFKL Pomeron is determined by the smallest transverse momentum, we conclude that in Fig. 14 the $Q_T$ dependence is determined by the function $N(Q_T)$. For the first two contributions to $N(Q_T)$ [see Fig. 11(a)], this is accurate to the order of $1/(R_N p_{T1})$. For the third contribution of the large mass diffraction, the accuracy is about $Q_s/p_{T1}$, where $Q_s$ denotes the saturation momentum of the BFKL Pomeron with rapidity $Y-y'$.

In spite of the fact that we indicate in Fig. 11(a) the sources of experimental information on each contribution, the situation turns out to be more complicated. As an example, we discuss the elastic contribution. This gives $N(Q_T) = g^2(Q_T)$, where $g(Q_T)$ is the Pomeron-hadron vertex. At first, we appear to be able to extract this vertex directly from the experimental values of $d\sigma_{el}/dt$. However, this is certainly not correct. Indeed, the BFKL Pomeron cannot explain the shrinkage of the diffraction peak which is seen experimentally and which gives almost half of the slope of the elastic cross section for the energy range $W =$ 40–7000 GeV [29]. In the only model [30] for the soft interaction at high energy that is based on the BFKL Pomeron and color glass condensate (CGC) approach [31,32], the effective shrinkage of the diffraction peak stems from strong shadowing corrections, which lead to an elastic amplitude that is different from that for the exchange of the BFKL Pomeron. However, it turns out that the most essential shadowing corrections originate from the BFKL Pomeron interaction of two scattering hadrons. Such corrections do not contribute to the inclusive cross sections nor to the correlation due to AGK cutting rules [20].

It turns out to be an even more complicated problem to extract, from the experimental data, the diffraction contribution to $N(Q_T)$ in the region of small masses. The lack of a theory, as well as insufficient experimental data, especially of the momentum transfer distribution of the

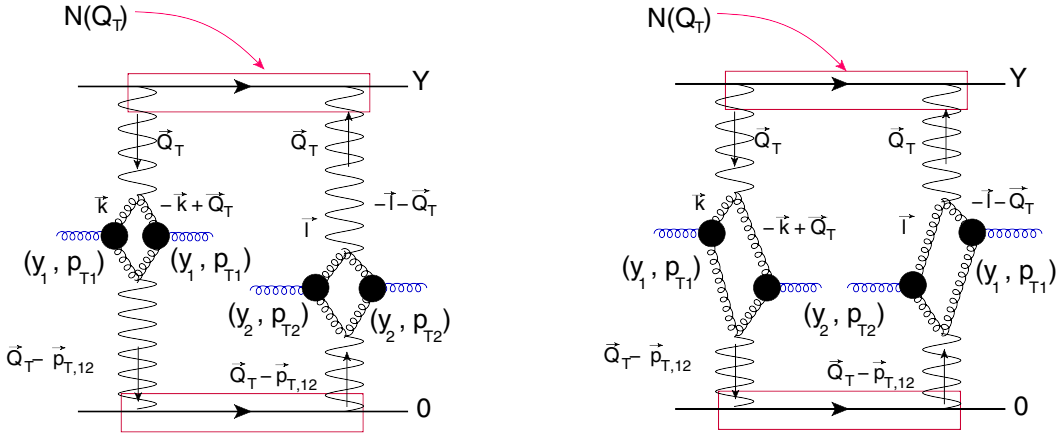


FIG. 14. The Mueller diagram for the double inclusive production of two gluons with rapidities $y_1$ and $y_2$ and transverse momenta $\boldsymbol{p}_{T1}$ and $\boldsymbol{p}_{T2}$ in the nucleon-nucleon interaction. The BFKL Pomerons are denoted by wavy lines. The first diagram corresponds to the square of the amplitude for two-parton-shower production, while the second diagram describes the interference.

diffractively produced state with fixed mass, leads to the necessity of modeling this process. The two extreme cases of such a modeling illustrate the difficulties: in our model [30] the rich variety of the produced states were replaced by a single state, and in the constituent quark model (CQM) [33] the small mass diffraction stems from production of the state of free three-constituent quarks. In our model the typical slope for $g_{\rm diff}(Q_T) \propto \exp(-BQ_T^2)$ turns out to be $1/4$ from the elastic slope, while in the CQM the size of the constituent quark is very small.

Taking the above into consideration, the uncertainties in the large mass diffraction term look small, and for the triple BFKL Pomeron vertex, both its value and transverse momentum dependence follow directly from the Balitsky-Kovchegov equation [31]. Bearing this in mind, we can write the expression for the interference diagram of Fig. 14 for the large mass diffraction contribution (see Fig. 11). As we have discussed in this case, $Q_T \sim Q_s(Y-y') \ll \min\{p_{T1}(p_{T2}), Q_s(y'-y_1)\}$, $|\boldsymbol{Q}_T - \boldsymbol{p}_{T,12}| \sim Q_s(Y-y') \ll \min\{p_{T1}(p_{T2}), Q_s(y'-y_1)\}$, and $k'_T \sim \min\{p_{T1}(p_{T2}), Q_s(y'-y_1)\}$ ($l'_T \sim \min\{p_{T1}(p_{T2}), Q_s(y'-y_1)\}$). Hence, we can use the factorized form for $\phi_N^G$ given by Eq. (A15) and Eq. (A16).

Finally, the large mass contribution for the interference diagram takes the form

$$
\begin{aligned}
&\frac{d^2\sigma}{dy_1 dy_2 d^2p_{T1} d^2p_{T2}}(\text{Fig.14, interference diagram}) \\
&= \frac{1}{2}\frac{1}{N_c^2-1}\left(\frac{2\pi\bar{\alpha}_S}{C_F}\right)^2 \frac{1}{p_{T1}^2 p_{T2}^2}\int dy' \int \phi_G^N(Y-y';Q_T=0;q_N,q'_T) \\
&\times \int d^2q'_T d^2k_T G^{\rm BFKL}\left(y'-y_1;Q_T;\boldsymbol{q}'_T-\frac{1}{2}\boldsymbol{Q}_T,k_T\right)\int dy'' G^{\rm BFKL}\left(y_2-y'';\boldsymbol{Q}_T-\boldsymbol{p}_{T,12};\boldsymbol{k}_T-\boldsymbol{p}_{T1},\boldsymbol{m}'_T-\frac{1}{2}(\boldsymbol{Q}_T-\boldsymbol{p}_{T,12})\right) \\
&\times \int d^2l_T d^2m'_T G^{\rm BFKL}\left(y'-y_1;Q_T,\boldsymbol{q}'_T+\frac{1}{2}\boldsymbol{Q}_T,l_T\right) G^{\rm BFKL}\left(y_2-y'';\boldsymbol{Q}_T-\boldsymbol{p}_{T,12};\boldsymbol{l}_T-\boldsymbol{p}_{T2},\boldsymbol{m}'_T+\frac{1}{2}(\boldsymbol{Q}_T-\boldsymbol{p}_{T,12})\right) \\
&\times \phi_G^N(y'';Q_T=0;m_N,m'_T).
\end{aligned}
\tag{46}
$$

In the diagram for the square of the amplitude we can put $\boldsymbol{p}_{T,12}=0$. Thus, the correlation function with the correlation length of the order of $1/Q_s(Y-y')$ takes the following form

$$
C(p_{T,12}/Q_s) = \frac{1}{2}\frac{1}{N_c^2-1}\frac{N}{D}, \tag{47}
$$

where

$$
\begin{aligned}
N &= \int d^2Q_T \int dy' \int \phi_G^N(Y-y';Q_T=0;q_N,q'_T) \\
&\times \int d^2q'_T d^2k_T G^{\rm BFKL}\left(y'-y_1;Q_T;\boldsymbol{q}'_T-\frac{1}{2}\boldsymbol{Q}_T,k_T\right)\int dy'' G^{\rm BFKL}\left(y_2-y'';\boldsymbol{Q}_T-\boldsymbol{p}_{T,12};\boldsymbol{k}_T-\boldsymbol{p}_{T1},\boldsymbol{m}'_T-\frac{1}{2}(\boldsymbol{Q}_T-\boldsymbol{p}_{T,12})\right) \\
&\times \int d^2l_T d^2m'_T G^{\rm BFKL}\left(y'-y_1;Q_T,\boldsymbol{q}'_T+\frac{1}{2}\boldsymbol{Q}_T,l_T\right) G^{\rm BFKL}\left(y_2-y'';\boldsymbol{Q}_T-\boldsymbol{p}_{T,12};\boldsymbol{l}_T-\boldsymbol{p}_{T2},\boldsymbol{m}'_T+\frac{1}{2}(\boldsymbol{Q}_T-\boldsymbol{p}_{T,12})\right) \\
&\times \phi_G^N(y'';Q_T=0;m_N,m'_T)
\end{aligned}
\tag{48}
$$

and

$$
\begin{aligned}
D &= \int d^2Q_T \int dy' \int \phi_G^N(Y-y';Q_T=0;q_N,q'_T) \\
&\times \int d^2q'_T d^2k_T \phi_G^N\left(y'-y_1;Q_T;\boldsymbol{q}'_T-\frac{1}{2}\boldsymbol{Q}_T,k_T\right)\int dy'' \phi_G^N\left(y_2-y'';\boldsymbol{Q}_T-\boldsymbol{p}_{T,12};\boldsymbol{k}_T-\boldsymbol{p}_{T1},\boldsymbol{m}'_T-\frac{1}{2}\boldsymbol{Q}_T\right) \\
&\times \int d^2l_T d^2m'_T \phi_G^N\left(y'-y_1;Q_T,\boldsymbol{q}'_T+\frac{1}{2}\boldsymbol{Q}_T,l_T\right)\phi_G^N\left(y_2-y'';\boldsymbol{Q}_T;\boldsymbol{l}_T,\boldsymbol{m}'_T+\frac{1}{2}\boldsymbol{Q}_T\right)\phi_G^N(y'';Q_T=0;m_N,m'_T).
\end{aligned}
\tag{49}
$$

The rather long algebraic expression of Eq. (48) and Eq. (49) can be simplified using Eq. (A17), and they take the following forms:

$$N = \int d^2Q_T \int dy' e^{2\omega(\frac{1}{2},0)y'} d^2q'_T \phi_G^N(Y-y';Q_T=0;q_N,q'_T) \frac{V_{\frac{1}{2}}(\boldsymbol{q}'_T,\boldsymbol{Q}_T-\frac{1}{2}\boldsymbol{p}_{T,12})V_{\frac{1}{2}}(\boldsymbol{q}'_T,\boldsymbol{Q}_T+\frac{1}{2}\boldsymbol{p}_{T,12})}{|\boldsymbol{Q}_T-\frac{1}{2}\boldsymbol{p}_{T,12}||\boldsymbol{Q}_T+\frac{1}{2}\boldsymbol{p}_{T,12}|}$$
$$\times \int dy'' e^{2\omega(\frac{1}{2},0)y''} d^2l'_T \phi_G^N(y'';Q_T=0;l_N,l'_T) \frac{V_{\frac{1}{2}}(\boldsymbol{l}'_T,\boldsymbol{Q}_T)V_{\frac{1}{2}}(\boldsymbol{l}'_T,\boldsymbol{Q}_T)}{Q_T^2}, \tag{50}$$

$$D = \int d^2Q_T \int dy' e^{2\omega(\frac{1}{2},0)y'} d^2q'_T \phi_G^N(Y-y';Q_T=0;q_N,q'_T) \frac{V_{\frac{1}{2}}(\boldsymbol{q}'_T,\boldsymbol{Q}_T)V_{\frac{1}{2}}(\boldsymbol{q}'_T,\boldsymbol{Q}_T)}{Q_T^2}$$
$$\times \int dy'' e^{2\omega(\frac{1}{2},0)y''} d^2l'_T \phi_G^N(y'';Q_T=0;l_N,l'_T) \frac{V_{\frac{1}{2}}(\boldsymbol{l}'_T,\boldsymbol{Q}_T)V_{\frac{1}{2}}(\boldsymbol{l}'_T,\boldsymbol{Q}_T)}{Q_T^2}. \tag{51}$$

## V. $\bar{\alpha}_S(y_1-y_2) \gg 1$

All our previous estimates were performed for small rapidity difference $\bar{\alpha}_S|y_1-y_2| \le 1$. In this section we discuss large rapidity differences ($\bar{\alpha}_S|y_1-y_2| \ge 1$). For simplicity, we consider only correlations with the typical length of the order of $R_D$. In other words, we discuss the generalization of Fig. 7 and Fig. 8 to the case of large $y_{12}=|y_1-y_2|$. This generalization is shown in Fig. 15 for the interference diagrams. The new features here are that at rapidity $y'_1 < y_1$, we need to emit an additional gluon and integrate over both its rapidity ($y'_1$) and its transferred momentum ($p'_{T1}$). Indeed, without this emission the ladder between rapidities $y'_1$ and $y'_2$ in Fig. 15(b) will be in the octet state of color $SU_3$. The main idea is that the principle contribution stems from $p'_{T1} \ll p_{T1}$. In this case the BFKL Pomeron between rapidities $y'_1$ and $y'_2$ has a momentum transfer which is equal to $p_{T1}$. After emission of two extra gluons with rapidities $y'_2$ and $y_2$, we obtain that the lower BFKL Pomeron has momentum transfer $p_{T,12}$, as in the right side of Fig. 8. In this diagram $Q_T \propto 1/R_D$ and can be put equal to zero in all parts of the diagrams, except $G(Q_T)$ and $G(\boldsymbol{Q}_T-\boldsymbol{p}_{T,12})$.

First, we need to integrate over $p'_{T1}$. The vertex of the emission is shown in Fig. 16, which can be written as

$$\bar{\alpha}_S^2 \Gamma_\mu(\boldsymbol{k}_T,\boldsymbol{p}_{T1})\Gamma_\mu(\boldsymbol{l}_T,\boldsymbol{p}_{T1}) \frac{1}{k'^2_T l'^2_T} \Gamma_\nu(\boldsymbol{k}'_T,\boldsymbol{p}_{T1})$$
$$\times \Gamma_\nu(\boldsymbol{l}'_T,\boldsymbol{p}_{T1}) \frac{1}{k''^2_T l''^2_T} \tag{52}$$

with $\boldsymbol{k}'_T=\boldsymbol{k}_T-\boldsymbol{p}_{T1}$ and $\boldsymbol{k}''_T=\boldsymbol{k}'_T-\boldsymbol{p}'_{T1}=\boldsymbol{k}_T-\boldsymbol{p}_{T1}-\boldsymbol{p}'_{T1}$. Plugging in Eq. (5), Eq. (6), and Eq. (26), one can see that Eq. (52) takes the form

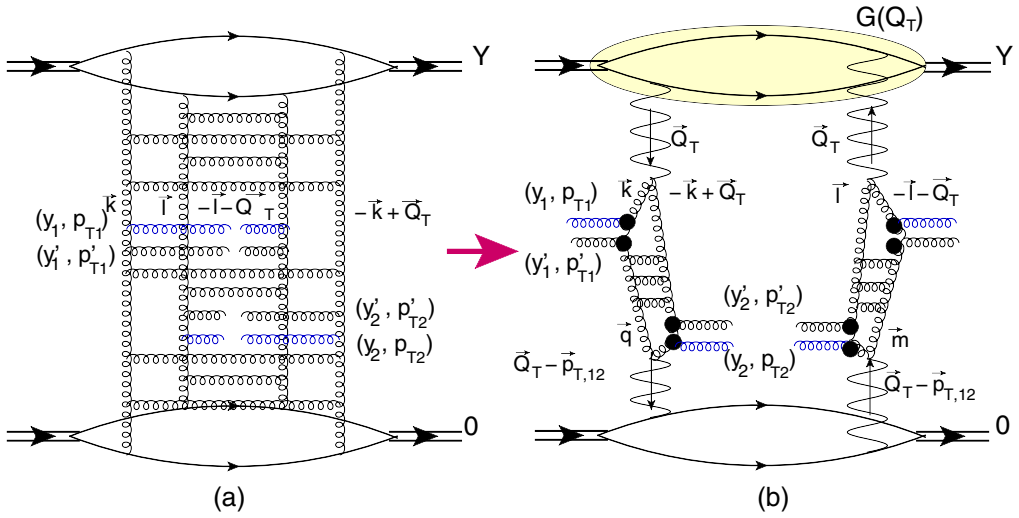


FIG. 15. The double inclusive production of two gluons with rapidities $y_1$ and $y_2$ in the case of large $|y_1-y_2|$ ( $\bar{\alpha}_S|y_1-y_2| \gg 1$) and transverse momenta $\boldsymbol{p}_{T1}$ and $\boldsymbol{p}_{T2}$ for the exchange of two BFKL Pomerons which are denoted by wavy lines. This diagram is the LLA generalization of Fig. 8. The solid lines denote nucleons in the deuterons, which are illustrated by double lines. Figure 15(a) describes the emission of extra gluons with rapidities $y_1 > y_i > y_2$. The ladder in Fig. 15(b) represents the BFKL Pomeron with the momentum transferred $\boldsymbol{p}_{T1}+\boldsymbol{p}'_{T1} \approx \boldsymbol{p}_{T1}$ for $p'_{T1} \ll p_{T2}$ (see the text).

$$\bar{\alpha}_S^2 \int d^2p'_{T1} \frac{1}{p'^2_{T1}} \left\{ \frac{k_T^2}{k'^2_T} + \frac{l_T^2}{l'^2_T} - \frac{p^2_{T1}}{k'^2_T l'^2_T} \right\} \frac{1}{p'^2_{T1}} \left\{ \frac{k'^2_T}{k''^2_T} + \frac{l'^2_T}{l''^2_T} - \frac{p'^2_{T1}}{k''^2_T l''^2_T} \right\}$$
$$\xrightarrow{p'_{T1} \ll k'_T (l'_T)} 2\bar{\alpha}_S^2 \int^{k'_T} \frac{d^2p'_{T1}}{p'^2_{T1}} \left[ \frac{1}{p^2_{T1}} \left\{ \frac{k_T^2}{k'^2_T} + \frac{l_T^2}{l'^2_T} - \frac{p^2_{T1}}{k'^2_T l'^2_T} \right\} \right]$$
$$= 2\bar{\alpha}_S^2 \int^{\min\{k'_T, l'_T\}} \frac{d^2p'_{T1}}{p'^2_{T1}} K(\boldsymbol{k}_T - \boldsymbol{l}_T, \boldsymbol{k}_T, \boldsymbol{k}'_T). \tag{53}$$

Note that the term [...] is the same as in Fig. 8 and $K(\boldsymbol{k}_T - \boldsymbol{l}_T, \boldsymbol{k}_T, \boldsymbol{k}'_T)$ is given by Eq. (27).

Finally, we obtain the following expression for the interference diagram of Fig. 16:

$$\frac{d^2\sigma}{dy_1 dy_2 d^2p_{T1} d^2p_{T2}}(\text{Fig.15} - \text{b})$$
$$= 2\left(\frac{2\pi\bar{\alpha}_S}{C_F}\right)^2 \bar{\alpha}_S^2 \int d^2Q_T G_D(Q_T) G_D(\boldsymbol{Q}_T - \boldsymbol{p}_{T,12}) \int d^2k_T \int d^2l_T \phi_G^N(Y - y_1; \boldsymbol{k}_T, -\boldsymbol{k}_T) \phi_G^N(Y - y_1; \boldsymbol{l}_T, -\boldsymbol{l}_T)$$
$$\times \int^{\min\{k'_T, l'_T\}} \int^{y_1} dy'_1 \frac{d^2p'_{T1}}{p'^2_{T1}} K(\boldsymbol{k}_T - \boldsymbol{l}_T, \boldsymbol{k}_T, \boldsymbol{k}'_T) \int_{y_2} dy'_2 \int^{\min\{q'_T, m'_T\}} \frac{d^2p'_{T2}}{p'^2_{T2}} K(\boldsymbol{q}_T - \boldsymbol{m}_T, \boldsymbol{q}_T, \boldsymbol{q}'_T)$$
$$\times \int d^2q_T \int d^2m_T G^{\text{BFKL}}(y'_1 - y'_2; \boldsymbol{p}_{T1}; \boldsymbol{k}'_T - \boldsymbol{p}'_{T1}, \boldsymbol{q}'_T + \boldsymbol{p}'_{T2}) G^{\text{BFKL}}(y'_1 - y'_2; -\boldsymbol{p}_{T1}; \boldsymbol{l}'_T - \boldsymbol{p}'_{T1}, \boldsymbol{m}'_T + \boldsymbol{p}'_{T2})$$
$$\times \phi_G^N(y_2; \boldsymbol{q}_T - \boldsymbol{p}_{T1}, -\boldsymbol{q}_T + \boldsymbol{p}_{T2}) \phi_G^N(y_2; \boldsymbol{m}_T, -\boldsymbol{m}_T). \tag{54}$$

In Eq. (54) we put $Q_T = 0$ everywhere, except in $G_D(Q_T)$ and $G_D(\boldsymbol{Q}_T - \boldsymbol{p}_{T,12})$, since $Q_T \sim 1/R_D \ll$ all other momenta. At first Eq. (54) appears to give a cross section which is suppressed as $\bar{\alpha}_S^2$ in comparison with Eq. (28). However, the integration over $y'_1$ and $y'_2$ leads to $1/\bar{\alpha}_S^2$ contributions, resulting in a cross section of the order of $\bar{\alpha}_S^2$. One can also see that the cross section does not depend on the rapidity difference $y_{12}$ for the large values of this difference.

The generalization to other cases, which we have considered above, is straightforward, and we do not discuss it here.

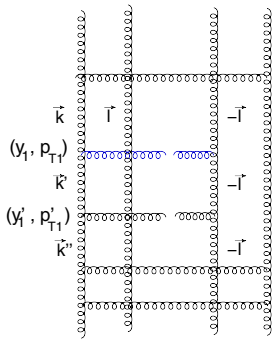


FIG. 16. The part of the diagram of Fig. 15(a) with the vertex of emission of two gluons.

## VI. CONCLUSIONS

### A. Comparison with other estimates in perturbative QCD

The first estimate of the azimuthal correlations due to the Bose-Einstein correlation in perturbative QCD was performed in Ref. [2] (see also Ref. [3]). The diagrams that were considered in these papers are shown in Fig. 17(a). The observation is that these diagrams give rather strong azimuthal correlations, but they are symmetric with respect to $\phi \to \pi - \phi$ and only generate $v_n$ with even $n$. The general origin of this symmetry was discussed in section II-B for slightly different diagrams. In Refs. [2,3] the $Q_T$ dependence was neglected, leading to $\delta$ function contributions which were smeared out by $Q_T$ dependance with $Q_T \sim 1/R$, where $R$ is the size of the interacting dipoles in Fig. 17(a).

Since Fig. 17(a) describes the production of two identical gluons in the dipole-dipole amplitude in the Born approximation of perturbative QCD, these diagrams are responsible for the azimuthal correlations in the one-parton cascade shown in Fig. 17(b). It is worthwhile to mention that the diagram of Fig. 17(a) leads to a contribution which is proportional to $\exp(-\omega(\frac{1}{2}, 0)y_{12})$ and describes the correlations that decrease for large $y_{12}$. Therefore, only for $\omega(\frac{1}{2}, 0)y_{12} \ll 1$ can we consider this diagram as a source of correlations which are independent of $y_{12}$.

Taking into account the emission of gluons, we can generalize the diagram of Fig. 17(a) to the diagram of Fig. 18. We have considered this diagram above and have

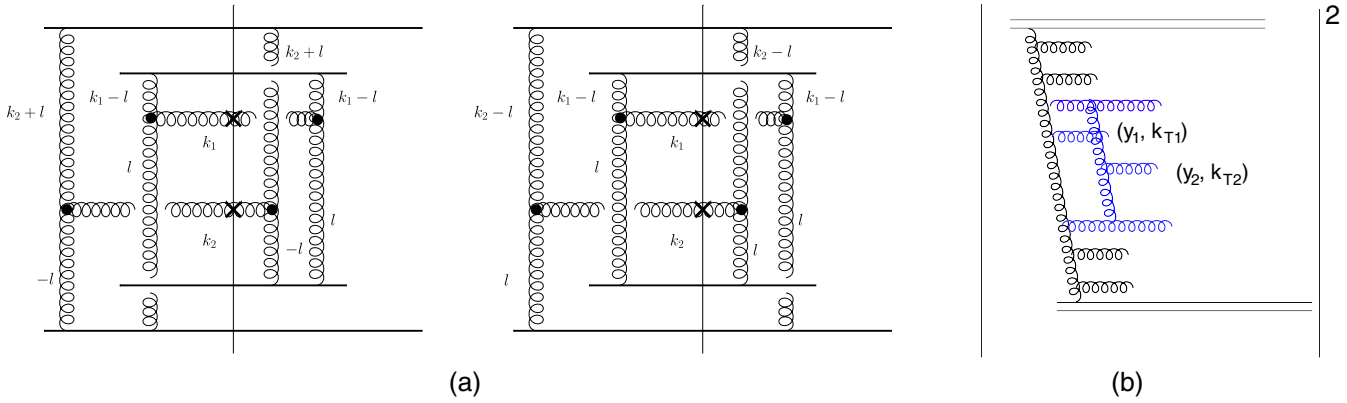


FIG. 17. Figure 17(a) is taken from Ref. [2] and describes the correlation in a one-parton shower. These correlations are shown in Fig. 17(b) in terms of gluon production in the single parton shower.

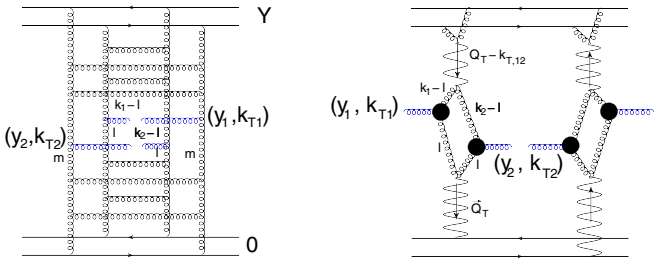


FIG. 18. The generalized diagram of Fig. 17(a), taking into account the gluon emission (two-parton-shower contribution).

shown that there is no symmetry with respect of $\phi \to \pi - \phi$ in such diagrams. Therefore, we conclude that the symmetry $\phi \to \pi - \phi$ is a feature of the azimuthal correlations in the one-parton shower in the Born approximation of perturbative QCD.

### B. Summary

In this paper, we found that, within the framework of perturbative QCD, the Bose-Einstein correlations due to two-parton-shower production induce azimuthal angle correlations with three correlation lengths: the size of the deuteron, the proton radius, and the size of the BFKL Pomeron, which is closely related to the saturation momentum ($R_c \sim 1/Q_s$). These correlations are independent of the values of rapidities of produced gluons (long range rapidity correlations) and have no symmetry with respect to $\phi \to \pi - \phi$ ($\boldsymbol{p}_{T1} \to -\boldsymbol{p}_{T1}$). Therefore, they give rise to $v_n$ for all values of $n$, not only for even values.

We reproduce the results of Refs. [2,3], which show this symmetry in the Born approximation of perturbative QCD. However, even in the Born approximation, this symmetry depends on the amplitude of the gluon-nucleon interaction at large distances of about the nucleon size; therefore, it inherently has a nonperturbative nature. Replacing the nucleon with an onium (the quark-antiquark bound state of heavy quarks), we see that symmetry $\phi \to \pi - \phi$ ($\boldsymbol{p}_{T1} \to -\boldsymbol{p}_{T1}$), does not hold for distances of the order of the size of the onium.

We demonstrated that the azimuthal correlations with the correlation length ($R_c$) of about the size of the deuteron and the size of nucleon stem from a nonperturbative contribution. Further, their estimates demand a lot of modeling due to the embryonic state of the theory in the nonperturbative region. However, the correlations with $R_c \sim 1/Q_s$ have a perturbative origin and can be evaluated in the framework of the CGC approach.

We showed that the two-parton-shower contributions generate long range rapidity azimuthal angle correlations, which intuitively have been expected. In other words, we demonstrated that the azimuthal angle correlations do not depend on $y_{12} = |y_1 - y_2|$ for large values of $y_{12}$ ($\bar{\alpha}_S y_{12} \geq 1$). We illustrated that the correlations of Refs. [2,3] actually describe the correlations in a one-parton shower and can be viewed, as they are independent of the rapidity difference only in the narrow rapidity window $\bar{\alpha}_S y_{12} \ll 1$.

## ACKNOWLEDGMENTS

We thank our colleagues at Tel Aviv University and UTFSM for encouraging discussions. Our special thanks go to Carlos Cantreras, Alex Kovner, and Michel Lublinsky for elucidating discussions on the subject of this paper. This research was supported by the BSF Grant No. 2012124, by Proyecto Basal FB 0821 (Chile), Fondecyt (Chile) Grant No. 1140842, and by CONICYT Grant No. PIA ACT1406.

## APPENDIX A: $Q_T$ DEPENDENCE OF THE BFKL POMERON

The impact parameter dependence of the BFKL Pomeron is well known [23], and it has the following form for the scattering of two dipoles ($r_1$ and $r_2$) at impact parameter $b$ [23,34]:

$$N_{\mathbb{P}}(r_1, r_2; Y, b) = \int \frac{d\gamma}{2\pi i} e^{\omega(\gamma,0)Y} H^{\gamma}(w, w^*), \qquad \text{(A1)}$$

where

$$\omega(\gamma,0)=\bar{\alpha}_S(2\psi(1)-\psi(\gamma)-\psi(1-\gamma)), \tag{A2}$$

and where $\psi(z)$ is the Euler $\psi(z)=d\ln\Gamma(z)/dz$ (digamma function) (see Ref. [35] formulas **8.360 – 8.367**).

$$\begin{aligned}&H^{\gamma}(w,w^*)\\&\equiv\frac{(\gamma-\frac{1}{2})^2}{(\gamma(1-\gamma))^2}\{b_\gamma w^\gamma w^{*\gamma}F(\gamma,\gamma,2\gamma,w)F(\gamma,\gamma,2\gamma,w^*)\\&+b_{1-\gamma}w^{1-\gamma}w^{*1-\gamma}F(1-\gamma,1-\gamma,2-2\gamma,w)\\&\times F(1-\gamma,1-\gamma,2-2\gamma,w^*)\}\end{aligned} \tag{A3}$$

$$\xrightarrow{ww^*\ll1}\frac{(\gamma-\frac{1}{2})^2}{(\gamma(1-\gamma))^2}\{b_\gamma w^\gamma w^{*\gamma}+b_{1-\gamma}w^{1-\gamma}w^{*1-\gamma}\}, \tag{A4}$$

where $F\equiv{}_2F_1$ is hypergeometric function [35]. In Eq. (A3) $ww^*$ is equal to

$$ww^*=\frac{r_1^2r_2^2}{(\boldsymbol{b}-\frac{1}{2}(\boldsymbol{r}_1-\boldsymbol{r}_2))^2(\boldsymbol{b}+\frac{1}{2}(\boldsymbol{r}_1-\boldsymbol{r}_2))^2}, \tag{A5}$$

and $b_\gamma$ is given by

$$b_\gamma=\pi^3 2^{4(1/2-\gamma)}\frac{\Gamma(\gamma)}{\Gamma(1/2-\gamma)}\frac{\Gamma(1-\gamma)}{\Gamma(1/2+\gamma)}. \tag{A6}$$

From Eq. (A3) and Eq. (A5) we see that (i) $b$ is about of the size of the largest dipole ($b\sim r_2$ for $r_2\gg r_1$), and (ii) the scattering amplitude has a symmetry with respect to $\boldsymbol{b}\to-\boldsymbol{b}$. $Q_T$ is the conjugate variable to $b$, and since

$$\begin{aligned}N_{\mathbb{P}}(r_1,r_2;b;Y)=r_1^2r_2^2\int d^2k d^2k' e^{i\boldsymbol{k}_T\cdot\boldsymbol{r}_1+i\boldsymbol{k}'_T\cdot\boldsymbol{r}_2}\\\times\int d^2Q_T e^{i\boldsymbol{Q}_T\cdot\boldsymbol{b}}G^{\rm BFKL}(Y;Q_T;k'_T,k_T),\end{aligned} \tag{A7}$$

we see that the value of typical $Q_T\propto1/r_2\approx1/R_N$. In Eq. (A7) $G^{\rm BFKL}(y-y';Q_T;k'_T,k_T)$ denotes the BFKL Pomeron Green function with the momentum transferred $Q_T$ and the transverse momenta of gluons $k_T$ at y and $k'_T$ at y'. The initial condition for the BFKL Green function is the exchange of two gluons at $y=y'$.

In Eq. (A7), the value of $r_1$ in our problem is about $1/p_{T1}$ or $1/p_{T2}$, and we trust perturbative QCD calculations only if $p_{T1}\sim p_{T2}\gg1/R_N$. Since $r_1\ll r_2$, we can use Eq. (A4) and take $ww^*$ to be equal to

$$ww^*=\frac{r_1^2r_2^2}{(\boldsymbol{b}-\frac{1}{2}\boldsymbol{r}_2)^2(\boldsymbol{b}+\frac{1}{2}\boldsymbol{r}_2)^2}. \tag{A8}$$

Bearing in mind that

$$I_\gamma(\boldsymbol{k})=\int\frac{d^2r}{(r^2)^\gamma}e^{i\boldsymbol{k}\cdot\boldsymbol{r}}=2^{1-2\gamma}\frac{\Gamma(1-\gamma)}{\Gamma(\gamma)}\frac{1}{(k^2)^{1-\gamma}}, \tag{A9}$$

by plugging Eq. (A9) into Eq. (A7), we obtain

$$\begin{aligned}G^{\rm BFKL}(\gamma;\boldsymbol{Q}_T;\boldsymbol{k'}_T,\boldsymbol{k}_T)=\frac{(\gamma-\frac{1}{2})^2}{(\gamma(1-\gamma))^2}\Big\{b_\gamma\int d^2m'_T I_{1-\gamma}(\boldsymbol{k'}_T-\boldsymbol{m'}_T)I_\gamma\Big(\boldsymbol{m'}-\frac{1}{2}\boldsymbol{Q}_T\Big)I_\gamma\Big(\boldsymbol{m'}+\frac{1}{2}\boldsymbol{Q}_T\Big)I_{1-\gamma}(\boldsymbol{k}_T)\\+b_{1-\gamma}\int d^2m_T I_\gamma(\boldsymbol{k'}_T-\boldsymbol{m}_T)I_{1-\gamma}\Big(\boldsymbol{m}-\frac{1}{2}\boldsymbol{Q}_T\Big)I_{1-\gamma}\Big(\boldsymbol{m}+\frac{1}{2}\boldsymbol{Q}_T\Big)I_\gamma(\boldsymbol{k}_T)\Big\}.\end{aligned} \tag{A10}$$

The integrals over $m'$ can be taken by replacing vector variables with the complex coordinates [23]

$$\boldsymbol{k}\to\rho_k=k_x+ik_y;\qquad\rho_k^*=k_x-ik_y, \tag{A11}$$

where $k_x$ and $k_y$ denote the $x$ and $y$ projections of $\boldsymbol{k}$. Using formula **3.197(1)** of Ref. [35], we can take integrals over $d^2m'=d\rho_{m'}d\rho^*_{m'}$, as follows:

$$\begin{aligned}V_\gamma(\boldsymbol{k'_T},\boldsymbol{Q}_T)&=\int d^2m'_T I_{1-\gamma}(\boldsymbol{k'}_T-\boldsymbol{m'}_T)I_\gamma\Big(\boldsymbol{m'}-\frac{1}{2}\boldsymbol{Q}_T\Big)I_\gamma\Big(\boldsymbol{m'}+\frac{1}{2}\boldsymbol{Q}_T\Big)\\&=\int d\rho_{m'}d\rho^*_{m'}I_{1-\gamma}((\rho_k-\rho_{m'}(\rho_k^*-\rho^*_{m'}))I_\gamma\Big(\Big(\rho_{m'}+\frac{1}{2}\rho_Q\Big)\Big(\rho^*_{m'}+\frac{1}{2}\rho^*_Q\Big)\Big)I_\gamma\Big(\Big(\rho_{m'}-\frac{1}{2}\rho_Q\Big)\Big(\rho^*_{m'}-\frac{1}{2}\rho^*_Q\Big)\Big)\\&=2^{2-4\gamma}\Gamma^4(1-\gamma)\frac{1}{((\boldsymbol{k}_T-\frac{1}{2}\boldsymbol{Q}_T)^2)^\gamma}\frac{1}{(Q_T^2)^{1-2\gamma}}F\Big(\gamma,\gamma,1,\frac{\rho_k+\frac{1}{2}\rho_Q}{\rho_k-\frac{1}{2}\rho_Q}\Big)F\Big(\gamma,\gamma,1,\frac{\rho^*_k+\frac{1}{2}\rho^*_Q}{\rho^*_k-\frac{1}{2}\rho^*_Q}\Big),\end{aligned} \tag{A12}$$

$$= (\mathbf{9.1311} \text{ of Ref. [31]}) 2^{2-4\gamma}\Gamma^4(1-\gamma)\frac{1}{(Q_T^2)^\gamma} F\left(\gamma, 1-\gamma, 1, \frac{\rho_k+\rho_Q}{\rho_Q}\right) F\left(\gamma, 1-\gamma, 1, \frac{\rho_k^*+\rho_Q^*}{\rho_Q^*}\right), \tag{A13}$$

$$\begin{aligned} &= (\mathbf{9.1322} \text{ of Ref. [31]}) 2^{2-4\gamma}\Gamma^4(1-\gamma)\frac{1}{((\boldsymbol{k}_T+\boldsymbol{Q}_T)^2)^\gamma} \\ &\times \left\{\frac{\Gamma(1-2\gamma)}{\Gamma^2(1-\gamma)} F\left(\gamma,\gamma,2\gamma,\frac{\rho_Q}{\rho_k+\rho_Q}\right) + \left(\frac{\rho_Q}{\rho_k+\rho_Q}\right)^{1-2\gamma}\frac{\Gamma(-1+2\gamma)}{\Gamma^2(1\gamma)} F\left(1-\gamma,1-\gamma,2(1-\gamma),\frac{\rho_Q}{\rho_k+\rho_Q}\right)\right\} \\ &\times \left\{\frac{\Gamma(1-2\gamma)}{\Gamma^2(1-\gamma)} F\left(\gamma,\gamma,2\gamma,\frac{\rho_Q^*}{\rho_k^*+\rho_Q^*}\right) + \left(\frac{\rho_Q^*}{\rho_k^*+\rho_Q^*}\right)^{1-2\gamma}\frac{\Gamma(-1+2\gamma)}{\Gamma^2(1\gamma)} F\left(1-\gamma,1-\gamma,2(1-\gamma),\frac{\rho*_Q}{\rho_k^*+\rho_Q^*}\right)\right\}. \end{aligned} \tag{A14}$$

Plugging Eq. (A11) into Eq. (A10), one can see that $\phi_G^N(\gamma, \boldsymbol{k'}_T, \boldsymbol{k}_T, \boldsymbol{Q}_T)$ can be written in the factorized form

$$\begin{aligned} G^{\mathrm{BFKL}}(\gamma; \boldsymbol{Q}_T; \boldsymbol{k'}_T, \boldsymbol{k}_T) &= V_\gamma(\boldsymbol{k'_T}, \boldsymbol{Q}_T) I_\gamma(\boldsymbol{k}_T) \\ &+ V_{1-\gamma}(\boldsymbol{k'_T}, \boldsymbol{Q}_T) I_{1-\gamma}(\boldsymbol{k}_T). \end{aligned} \tag{A15}$$

$\phi_G^N$ in the rapidity representation can be calculated as

$$\begin{aligned} &G^{\mathrm{BFKL}}(Y;, \boldsymbol{Q}_T; \boldsymbol{k'}_T, \boldsymbol{k}_T) \\ &= \int_{\epsilon-i\infty}^{\epsilon+i\infty} \frac{d\gamma}{2\pi i} e^{\omega(\gamma,0)Y} G^{\mathrm{BFKL}}(\gamma, \boldsymbol{k'}_T, \boldsymbol{k}_T, \boldsymbol{Q}_T). \end{aligned} \tag{A16}$$

Taking the integral over $\gamma$ in Eq. (A16) by the method of steepest descent [18], we see that for large $Y \gg 1$ the essential $\gamma = \frac{1}{2} + i\nu$, where $\nu$ is small. Bearing this in mind, we can see from Eq. (A13) that at large $Q_T \gg k'_T$, $G^{\mathrm{BFKL}}(Y;, \boldsymbol{Q}_T; \boldsymbol{k'}_T, \boldsymbol{k}_T) \propto 1/(Q_T^2)^\gamma \approx 1/Q_T$. At $Q_T \to 0 Q_T \gg k'_T G^{\mathrm{BFKL}}(Y;, \boldsymbol{Q}_T; \boldsymbol{k'}_T, \boldsymbol{k}_T) \to$ Const. Therefore, we conclude that the typical value $Q_T$ in the BFKL Pomeron is about $k'_T$, the smallest transverse momenta.

At large $Y$ we can simplify Eq. (A16) using Eq. (A15) and the small size of $\nu$. Plugging $G^{\mathrm{BFKL}}(Y;, \boldsymbol{Q}_T; \boldsymbol{k'}_T, \boldsymbol{k}_T)$ from Eq. (A15) into Eq. (A16), we have

$$\begin{aligned} &G^{\mathrm{BFKL}}(Y; \boldsymbol{Q}_T; \boldsymbol{k'}_T, \boldsymbol{k}_T) \\ &= \int_{\epsilon-i\infty}^{\epsilon+i\infty} \frac{d\gamma}{2\pi i} e^{\omega(\gamma,0)Y} 2V_{\frac{1}{2}+i\nu}(\boldsymbol{k'_T}, \boldsymbol{Q}_T) I_\gamma(\boldsymbol{k}_T) \\ &\xrightarrow{\nu \ll 1} \frac{2C(\gamma=\frac{1}{2})}{k'_T k_T} V_{\frac{1}{2}}(\boldsymbol{k'_T}, \boldsymbol{Q}_T) \\ &\times \int_{-\infty+i\epsilon}^{+\infty+i\epsilon} \frac{d\nu}{2\pi} e^{(\omega(\frac{1}{2},0)-D\nu^2)Y + i\nu \ln(k_T^2/k'^2_T)} \\ &= \frac{2C(\gamma=\frac{1}{2})}{k'_T k_T} V_{\frac{1}{2}}(\boldsymbol{k'_T}, \boldsymbol{Q}_T) \left(\sqrt{\frac{2\pi}{DY}} e^{\omega(\frac{1}{2},0)Y - \frac{\ln^2(k'^2_T/k_T^2)}{4DY}}\right). \end{aligned} \tag{A17}$$

The integral in Eq. (A17) is taken in the saddle point approximation with $\nu_{SP} = i \ln(k_T^2/k'^2_T)/2DY \ll 1$ and $\omega(\frac{1}{2} = i\nu, 0) = \omega(\frac{1}{2}, 0) - D\nu^2$.

## APPENDIX B: THE BFKL POMERON-ONIUM VERTEX

The scattering amplitude of a dipole of size $x_{01}$ with an onium has the following form:

$$\begin{aligned} A(Y, x_{01}; Q_T) = &\int d^2x'_{01} e^{i\boldsymbol{x}'_{01}\cdot\boldsymbol{Q}_T} \Psi^*_{\mathrm{onium}}(x'_{01}) \\ &\times N(Y; x'_{01}, x_{01}, Q_T) \Psi^*_{\mathrm{onium}}(x'_{01}). \end{aligned} \tag{B1}$$

In the momentum representation it can be written as

$$\begin{aligned} &A(\gamma, k'_T, k_T, Q_T) \\ &= (F(Q_T) - F(2\boldsymbol{k'}_T - \boldsymbol{Q}_T)) \\ &\times \int d^2x'_{01} e^{-i\boldsymbol{k'}_T\cdot\boldsymbol{x}'_{01} - i\boldsymbol{k}_T\cdot\boldsymbol{x}_{01}} N(\gamma; x'_{01}, x_{01}, Q_T)/x_{01}^2. \end{aligned} \tag{B2}$$

The amplitude $e^{-i\boldsymbol{k'}_T\cdot\boldsymbol{x}'_{01} - i\boldsymbol{k}_T\cdot\boldsymbol{x}_{01}} N(\gamma; x'_{01}, x_{01}, Q_T)/x_{01}^2$ can be written in the factorized form of Eq. (A15)

$$\begin{aligned} &e^{-i\boldsymbol{k'}_T\cdot\boldsymbol{x}'_{01} - i\boldsymbol{k}_T\cdot\boldsymbol{x}_{01}} N(\gamma; x'_{01}, x_{01}, Q_T)/x_{01}^2 \\ &= V^{\mathrm{pr}}_\gamma(\boldsymbol{k'_T}, \boldsymbol{Q}_T) N_\gamma(\boldsymbol{k}_T) + V^{\mathrm{pr}}_{1-\gamma}(\boldsymbol{k'_T}, \boldsymbol{Q}_T) N_{1-\gamma}(\boldsymbol{k}_T), \end{aligned} \tag{B3}$$

where $V^{\mathrm{pr}}_\gamma(\boldsymbol{k'_T}, \boldsymbol{Q}_T)$ is equal to

$$V^{\rm pr}_{\gamma}(\boldsymbol{k'_T},\boldsymbol{Q}_T) = \int d^2m'_T I_{-\gamma}(\boldsymbol{k'}_T-\boldsymbol{m'}_T) I_{\gamma}\left(\boldsymbol{m'}-\frac{1}{2}\boldsymbol{Q}_T\right) I_{\gamma}\left(\boldsymbol{m'}+\frac{1}{2}\boldsymbol{Q}_T\right)$$
$$= \int d\rho_{m'} d\rho^*_{m'} I_{-\gamma}((\rho_k-\rho_{m'}(\rho^*_k-\rho^*_{m'}))) I_{\gamma}\left(\left(\rho_{m'}+\frac{1}{2}\rho_Q\right)\left(\rho^*_{m'}+\frac{1}{2}\rho^*_Q\right)\right) I_{\gamma}\left(\left(\rho_{m'}-\frac{1}{2}\rho_Q\right)\left(\rho^*_{m'}-\frac{1}{2}\rho^*_Q\right)\right)$$
$$= 2^{3-2\gamma}\frac{\Gamma(1+\gamma)\Gamma^2(1-\gamma)}{\Gamma(-\gamma)\Gamma^2(\gamma)}\frac{1}{((\boldsymbol{k}_T-\frac{1}{2}\boldsymbol{Q}_T)^2)^{1+\gamma}}\frac{1}{(Q^2_T)^{1-2\gamma}} F\left(1+\gamma,\gamma,2,\frac{\rho_k+\frac{1}{2}\rho_Q}{\rho_k-\frac{1}{2}\rho_Q}\right) F\left(1+\gamma,\gamma,2,\frac{\rho^*_k+\frac{1}{2}\rho^*_Q}{\rho^*_k-\frac{1}{2}\rho^*_Q}\right). \tag{B4}$$

Finally, the BFKL Pomeron-onium vertex takes the form

$$V^{\rm onium}_{\gamma}(Q_T) = \int d^2k'_T (F(Q_T)-F(2\boldsymbol{k'}_T-\boldsymbol{Q}_T)) V^{\rm pr}_{\gamma}(\boldsymbol{k'_T},\boldsymbol{Q}_T). \tag{B5}$$


[1] E. M. Levin, M. G. Ryskin, and S. I. Troian, Yad. Fiz. **23**, 423 (1976) [Sov. J. Nucl. Phys. **23**, 222 (1976)]; A. Capella, A. Krzywicki, and E. M. Levin, Phys. Rev. D **44**, 704 (1991).

[2] Y. V. Kovchegov and D. E. Wertepny, Nucl. Phys. **A906**, 50 (2013).

[3] T. Altinoluk, N. Armesto, G. Beuf, A. Kovner, and M. Lublinsky, Phys. Lett. B **752**, 113 (2016); **751**, 448 (2015).

[4] E. Gotsman, E. Levin, and U. Maor, arXiv:1604.04461; Eur. Phys. J. C **76**, 607 (2016).

[5] V. Khachatryan *et al.* (CMS Collaboration), Phys. Rev. Lett. **116**, 172302 (2016); J. High Energy Phys. 09 (2010) 091.

[6] J. Adams *et al.* (STAR Collaboration), Phys. Rev. Lett. **95**, 152301 (2005).

[7] B. Alver *et al.* (PHOBOS Collaboration), Phys. Rev. Lett. **104**, 062301 (2010).

[8] H. Agakishiev *et al.* (STAR Collaboration), arXiv: 1010.0690.

[9] S. Chatrchyan *et al.* (CMS Collaboration), Phys. Lett. B **718**, 795 (2013); V. Khachatryan *et al.* (CMS Collaboration), J. High Energy Phys. 09 (2010) 091.

[10] S. Chatrchyan *et al.* (CMS Collaboration), J. High Energy Phys. 02 (2014) 088; Phys. Rev. C **89**, 044906 (2014); Eur. Phys. J. C **72**, 2012 (2012); J. High Energy Phys. 02 (2014) 088.

[11] J. Adam *et al.* (ALICE Collaboration), Phys. Rev. Lett. **116**, 132302 (2016); **117**, 182301 (2016); L. Milano (ALICE Collaboration), Nucl. Phys. **A931**, 1017 (2014); Y. Zhou (ALICE Collaboration), J. Phys. Conf. Ser. **509**, 012029 (2014).

[12] B. B. Abelev *et al.* (ALICE Collaboration), Phys. Rev. C **90**, 054901 (2014); Phys. Lett. B **726**, 164 (2013); B. Abelev *et al.* (ALICE Collaboration), Phys. Lett. B **719**, 29 (2013).

[13] G. Aad *et al.* (ATLAS Collaboration), Phys. Rev. Lett. **116**, 172301 (2016).

[14] G. Aad *et al.* (ATLAS Collaboration), Phys. Rev. C **90**, 044906 (2014); arXiv:1409.1792; B. Wosiek (ATLAS Collaboration), Ann. Phys. (Amsterdam) **352**, 117 (2015); G. Aad *et al.* (ATLAS Collaboration), Phys. Lett. B **725**, 60 (2013).

[15] B. Wosiek (ATLAS Collaboration), Phys. Rev. C **86**, 014907 (2012).

[16] R. Hanbury Brown and R. Q. Twiss, Nature (London) **178**, 1046 (1956).

[17] G. Goldhaber, W. B. Fowler, S. Goldhaber, and T. F. Hoang, Phys. Rev. Lett. **3**, 181 (1959); G. I. Kopylov and M. I. Podgoretsky, Yad. Fiz. **15**, 392 (1972) [Sov. J. Nucl. Phys. **15**, 219 (1972)]; G. Alexander, Rep. Prog. Phys. **66**, 481 (2003).

[18] Y. V. Kovchegov and E. Levin, *Quantum Chromodynamics at High Energies*, Cambridge Monographs on Particle Physics, Nuclear Physics and Cosmology (Cambridge University Press, Cambridge, England, 2012).

[19] R. J. Glauber, in *Lectures in Theoretical Physics*, edited by W. E. Brittin and L. G. Duham (Interscience, New York, 1959), Vol. 1.

[20] V. A. Abramovsky, V. N. Gribov, and O. V. Kancheli, Yad. Fiz. **18**, 595 (1973) [Sov. J. Nucl. Phys. **18**, 308 (1974)].

[21] E. Levin and A. H. Rezaeian, Phys. Rev. D **84**, 034031 (2011).

[22] E. A. Kuraev, L. N. Lipatov, and F. S. Fadin, Sov. Phys. JETP **45**, 199 (1977); Y. Y. Balitsky and L. N. Lipatov, Sov. J. Nucl. Phys. **28**, 22 (1978).

[23] L. N. Lipatov, Phys. Rep. **286**, 131 (1997); Sov. Phys. JETP **63**, 904 (1986), and references therein.

[24] A. H. Mueller, Phys. Rev. D **2**, 2963 (1970).

[25] V. N. Gribov, Zh. Eksp. Teor. Fiz. **53** (1967) 654 [Sov. Phys. JETP **26**, 414 (1968)].

[26] L. V. Gribov, E. M. Levin, and M. G. Ryskin, Phys. Rep. **100**, 1 (1983).

[27] M. A. Braun, Phys. Lett. B **632**, 297 (2006); Eur. Phys. J. C **48**, 511 (2006)]; arXiv:hep-ph/0504002; Eur. Phys. J. C **16**, 337 (2000).

[28] M. Kozlov, E. Levin, and A. Prygarin, Nucl. Phys. **A792**, 122 (2007).

[29] F. Ferro (TOTEM Collaboration), AIP Conf. Proc. **1350**, 172 (2011); G. Antchev *et al.* (TOTEM Collaboration), Europhys. Lett. **95**, 41001 (2011); **96**, 21002 (2011); Phys. Rev. Lett. **111**, 262001 (2013).

[30] E. Gotsman, E. Levin, and U. Maor, Eur. Phys. J. C **75**, 179 (2015); **75**, 18 (2015); Phys. Lett. B **746**, 154 (2015); Eur. Phys. J. C **75**, 518 (2015).

[31] I. Balitsky, Nucl. Phys. **B463**, 99 (1996); Phys. Rev. D **60**, 014020 (1999); Y. V. Kovchegov, Phys. Rev. D **60**, 034008 (1999).

[32] J. Jalilian-Marian, A. Kovner, A. Leonidov, and H. Weigert, Phys. Rev. D **59**, 014014 (1998); Nucl. Phys. **B504**, 415 (1997); J. Jalilian-Marian, A. Kovner, and H. Weigert, Phys. Rev. D **59**, 014015 (1998); A. Kovner, J. G. Milhano, and H. Weigert, Phys. Rev. D **62**, 114005 (2000); E. Iancu, A. Leonidov, and L. D. McLerran, Phys. Lett. B **510**, 133 (2001); Nucl. Phys. **A692**, 583 (2001); E. Ferreiro, E. Iancu, A. Leonidov, and L. McLerran, Nucl. Phys. **A703**, 489 (2002); H. Weigert, Nucl. Phys. **A703**, 823 (2002).

[33] Y. M. Shabelski and A. G. Shuvaev, Eur. Phys. J. C **75**, 438 (2015); J. High Energy Phys. 11 (2014) 023; S. Bondarenko and E. Levin, Eur. Phys. J. C **51**, 659 (2007); S. Bondarenko, E. Levin, and J. Nyiri, Eur. Phys. J. C **25**, 277 (2002); J. J. J. Kokkedee, *The Quark Model* (Benjamin, New York, 1969), and references therein; H. J. Lipkin and F. Scheck, Phys. Rev. Lett. **16**, 71 (1966); E. M. Levin and L. L. Frankfurt, JETP Lett. **2**, 65 (1965).

[34] H. Navelet and R. B. Peschanski, Nucl. Phys. **B507**, 353 (1997); Phys. Rev. Lett. **82**, 1370 (1999); Nucl. Phys. **B634**, 291 (2002).

[35] I. Gradstein and I. Ryzhik, *Table of Integrals, Series, and Products* (Academic Press, London, 1994), fifth ed.